RAPID DETECTION OF PESTICIDE RESIDUES IN FOODS USING SURFACE-ENHANCED RAMAN SPECTROSCOPY COUPLED WITH GOLD NANOSTARS

A Thesis

presented to

the Faculty of the Graduate School

at the University of Missouri

In Partial Fulfillment

of the Requirements for the Degree

Master of Science

by

Min-Hui Lin

Dr. Mengshi Lin, Thesis Supervisor

DECEMBER 2020

The undersigned, appointed by the dean of the Graduate School, have examined the thesis entitled

RAPID DETECTION OF PESTICIDE RESIDUES IN FOODS USING SURFACE-ENHANCED RAMAN SPECTROSCOPY COUPLED WITH GOLD NANOSTARS

presented by Min-Hui Lin,

a candidate for the degree of Master of Science,

and hereby certify that, in their opinion, it is worthy of acceptance.

_____

Dr. Mengshi Lin, Food Science

_____

Dr. Kiruba Krishnaswamy, Food Science

_____

Dr. Yangchuan Xing, Chemical Engineering

ACKNOWLEDGEMENTS

First, I would like to thank my advisor, Dr. Mengshi Lin, who gave me the precious opportunity to study Food Science at the University of Missouri and join his research group. He is approachable, kind, and patient in guiding me for my entire journey of my Master's program. I am grateful for his insightful guidance and warm support. I want to thank Dr. Kiruba Krishnaswamy and Dr. Yangchuan Xing for willingness to serve on my committee and providing professional advice. I also want to thank Drs. Azlin Mustapha, Andrew Clarke, Bongkosh Vardhanabhuti, and Ingolf Gruen for their passionate teaching and assistance along the way.

I would also like to thank my fellow graduate students and my lab colleagues, Sun Lin, Ezgi Tekin Pulatsu, and Sara Asgari, for their generous help and warm encouragement. I especially want to thank Sun Lin, who shared me with her firsthand knowledge and taught me laboratory skills. I feel privileged to study at MU and have the valuable chance to meet these wonderful people, who come from different places of the world.

Last but not the least, I am deeply grateful to my family and friends for their relentless love and support.

TABLE OF CONTENTS

LIST OF FIGURES

LIST OF TABLES

RAPID DETECTION OF PESTICIDE RESIDUES IN FOODS USING SURFACE-ENHANCED RAMAN SPECTROSCOPY COUPLED WITH GOLD NANOSTARS

Min-Hui Lin

Dr. Mengshi Lin, Thesis Supervisor

ABSTRACT

Constant monitoring pesticide residues in foods is an essential part of food safety. In recent years, there is a growing concern about food issues in agricultural products. Tradition testing methods such as high-performance liquid chromatography (HPLC) and gas chromatography–mass spectrometry (GC-MS) demand time-consuming sample preparations and well-trained operators. Therefore, this research aimed to establish a novel, simple, and rapid testing technique. In this study, the SERS performance of gold nanostars was evaluated by detecting two commonly used pesticides, thiabendazole (TBZ) and paraquat in the real food samples. Gold nanostars were used as a surface-enhanced Raman spectroscopy (SERS) substrate due to their highly branched structure, which provide many SERS hot spots for generating intensified Raman signals from the target analytes. Additionally, the rough topography of gold nanostars has large surface area, which can enable good interactions between the substrate and analyte molecules. The UV-vis spectrometer, electron microscopes and Zetasizer were utilized for characterization. The detection limits of this SERS method are 5 ppm for TBZ in apple juice and 0.2 ppm for paraquat in green tea. These results indicate that SERS coupled with gold nanostars is a

facile approach and has great potential to be applied for qualification and quantification of trace contaminants in foods.

CHAPTER 1

INTRODUCTION

1.1 Background

Food safety has attracted growing attention owing to frequent occurrences of food safety issues in recent years. In 2008, melamine-tainted milk products caused about 300,000 cases of illness and six babies died in China (Sharma & Paradakar, 2010). In 2010, foodborne disease associated with Shiga toxin-producing *E. coli* (STEC) sickened over one million people and killed at least 100 according to the estimation by the World Health Organization (WHO) (Pires et al., 2019). In 2011 in Taiwan, a slew of beverages were found contaminated with phthalate-adulterated clouding agents, which were misused to prolong shelf life and maximize profits (Yen et al., 2011). Between 2017 and 2018, more than 600 listeriosis cases were reported in South Africa (Boatemaa et al., 2019). A paper published on 2020 showed around 73% Cambodian and 100% Vietnamese famers included in the survey excessively used pesticides (Schreinemachers et al., 2020).

The afore-mentioned examples highlight the importance of food safety. In general, food hazards can be categorized into three classes—physical hazards, chemical hazards, and biological hazards. Physical hazards are associated with presences of foreign objects in food and can result in injury, illness, and customer dissatisfaction (Djekic et al., 2017). Chemical hazards arise from contamination of chemical substances including but not limited to sanitizers, machines oil, veterinary drugs, and pesticides. Biological hazards

usually involve pathogenic viruses, bacteria, fungi, or parasites, which can harm human health and cause foodborne illness outbreaks.

Among all the hazards, the adverse impacts result from the abuse of pesticides cannot be ignored. Pesticides, including herbicides, fungicides, and insecticides, are crucial in farming practices for the purpose of improving production and quality and preserving the freshness of fruits and vegetables. Rising pest infestations, which are caused by global warming, and growing world human population lead to higher demand for pesticide usage (Ahmad et al., 2019; Jallow et al., 2017). Nevertheless, some studies pointed out pesticide overuse are especially prevalent in developing countries (Bhandari et al., 2019; Donkor et al., 2016; Jallow et al., 2017; Zhang et al., 2015). Misuse of pesticides poses threats not only to the environment but also to public health (Narenderan et al., 2020). Moreover, previous research found that pesticide residues can be easily found in food products (Mahmood et al. 2015).

Thiabendazole (TBZ), a derivative of benzimidazole, is a broad-spectrum and widely utilized fungicide, which prevents the growth of spores and slows down fungal decay (Allen & Gottlieb, 1970). TBZ can be absorbed by plant tissues, suggesting potential risks of pesticide residues remaining even after TBZ treated surfaces has been rinsed (Yang et al., 2016). Furthermore, exposure to TBZ can lead to hepatic, renal impairments, and birth defects in humans (Jamieson et al., 2011).

Paraquat is one of the most used herbicides to increase planation yields by killing weeds through the interference of electron transfer of photosynthesis (Sétif, 2015). It was first marketed in the 1960's and has been commonly applied in agriculture and horticulture because of its inexpensiveness and nonselective feature (Huang et al., 2019). Over 100 nations worldwide allow the use of paraquat (Rashidipour et al., 2019), and it has been used for a huge variety of produce. However, the widespread applications increase the risks for bioaccumulation and detrimental impacts on soil microbes and ecosystems (Frimpong et al., 2018). In addition, paraquat is extremely poisonous to humans and its toxicity results from its ability to cause free radicals, which can further induce oxidative stress (Botta et al., 2020; Gawarammana & Buckley, 2011). Unfortunately, treating paraquat poisoning remains a challenge. Depending on the route and amount of exposure, paraquat can cause pulmonary edema and damage organs such as heart, liver, and kidney.

Government agencies and organizations around the world have established maximum residue levels (MRL) for pesticides to protect consumer health. The limits are typically set at parts per million (ppm) or parts per billion (ppb) levels. To monitor safety and quality of food commodities, regular analyses are performed by the food industry, testing laboratories, and regulatory entities. High performance liquid chromatography (HPLC) and gas chromatography–mass spectrometry (GC-MS) are popular analytical techniques to detect trace elements in foods (Bala et al., 2017). Although these methods are sensitive, they are expensive and required laborious sample preparations and well-trained technicians for operation (Singh et al., 2020; Zhu et al., 2017). Therefore, numerous efforts have been

dedicated to developing novel technology for trace analyses (Hongmei et al., 2020; Li et al., 2016; Xu et al., 2020).

Surface-enhanced Raman spectroscopy (SERS) is a powerful tool that can achieve high sensitivity. It was first discovered in the 1970's and gained attentions from researchers in various disciplines (Jeanmaire & Van Duyne, 1977). Raman signals are in essence weak but can be vastly enhanced by SERS substrates, which usually consist of metallic nanoscale motifs. High enhancement of Raman signals is usually achieved by excitation of collective electron oscillation within the nanostructure, leading to enormously amplification of the local electromagnetic fields. The phenomenon is known as electromagnetic enhancement. Another form of Raman enhancement called chemical enhancement is usually less significant and associated with electron transfer between target molecules and metallic elements. The electron interaction can increase molecule polarizability and consequently intensifies Raman signals (Tiwari et al., 2007).

Gold is classified as a noble metal and has high electron mobility. Gold nanoparticles strongly absorb and scatter light at visible and near infrared region and demonstrate localized plasmonic resonance, which increases local fields (Cognet & Lounis, 2008; Ghosh et al., 2017) As a result, gold nanoparticles are widely used components for SERS substrates.

Raman enhancement is greatly influenced by the properties of SERS substrates. Over the past few decades, varying material types, sizes, and forms of SERS substrates have been fabricated. It is known that shapes of nanoparticles can affect SERS performance because different shapes give rise to different resonant frequencies (Frederix et al., 2003). Hot spots, where strong enhancement occur by magnifying the local fields, can be created by forming metallic close gaps and sharp tips (Alvarez-Puebla et al., 2010).

The structure of gold nanostars is composed of a core and multiple outwardly protruding branches. Metaphorically speaking, the core of a nanostar is like an electron repository and vertices of stars serve as confiners focalizing the local fields when illuminated by light of desirable frequency (Rodríguez-Lorenzo et al., 2010). As a result, gold nanostars can be excellent SERS substrates and used for trace detection.

1.2 Objectives

The objectives of this study are as follows.

I. Characterizing gold nanostars with transmission electron microscope (TEM), scanning electron microscope (SEM), energy-dispersive X-ray spectroscopy (EDS), and Zetasizer

II. Using rhodamine 6G (R6G) to investigate the SERS performance of gold nanostars

III. Using gold nanostars as SERS substrates to detect thiabendazole (TBZ) in apple juice

IV. Using gold nanostars as SERS substrates to detect paraquat in green tea

CHAPTER 2

LITERATURE REVIEW

2.1 Raman spectroscopy

Raman spectroscopy is considered a vibrational spectroscopy, which depends on interactions between light and substances to obtain molecular vibrational modes and can be utilized for qualitative and quantitative analyses (Vagenas et al., 2003). It is well known that C. V. Raman and K. S. Krishnan first discovered Raman scattering (Qin et al., 2019).

The monochromatic light of a Raman instrument is used to excite the analyte molecules to acquired Raman signals. Different types of scattering can occur after excitation —Rayleigh, Stoke, and anti-Stoke scattering (Figure 2.1). Rayleigh scattering is elastic scattering, meaning that the energy of the incident photon is equivalent to that of the scattered photon. Hence, the analyte molecules do not gain or lose energy during the process. On the other hand, Stokes and anti-Stokes scatterings are defined as Raman scattering. In contrast to elastic scattering, Stokes and anti-Stokes scatterings are accompanied with energy transfer between the photons and molecules, thus providing vibrational information of the molecules (Ember et al., 2017)

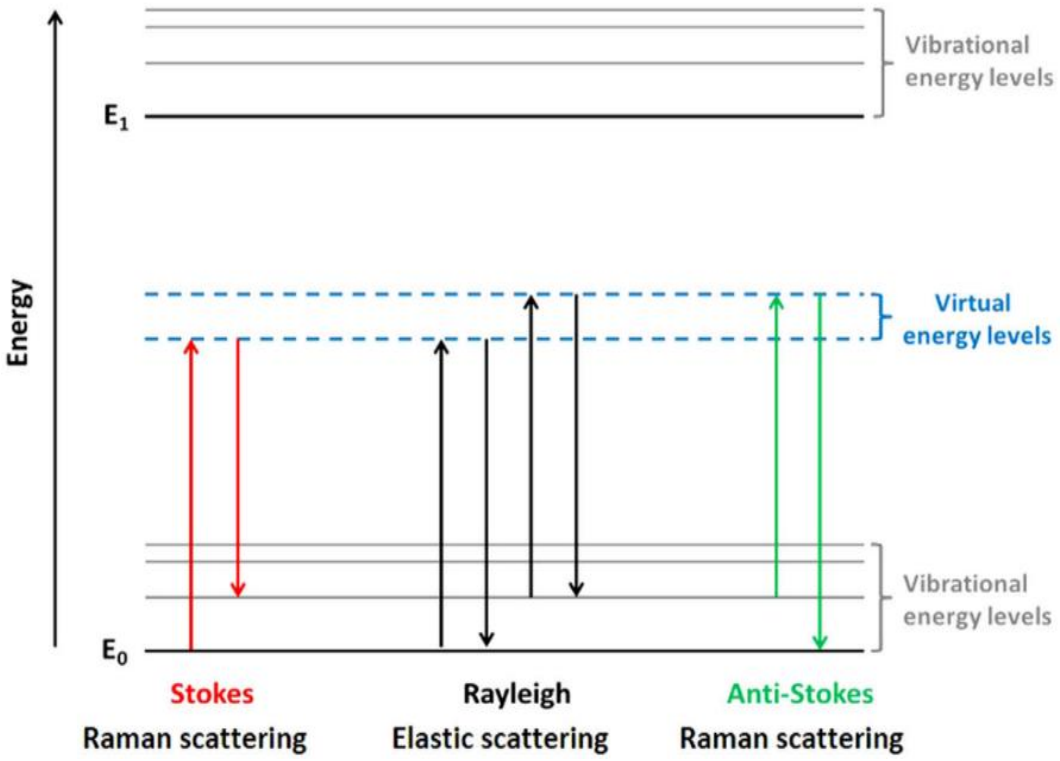

Figure 2.1. Illustration of different types of scatterings (Ember et al. 2017).

During the Stokes process, the molecules absorb energy from the incident photons and therefore excited from a ground state to a higher energy vibrational state. However, in the anti-Stokes process, the molecules are at virtual state in the beginning owing to the thermal energy and the energy is transferred from the molecules to the photons. Because, in most cases, the molecules are at ground state, the intensity of anti-Stokes scattering is feeble. Raman shift is the energy difference between the incident photon and scattered photon. Stokes events have positive Raman shift, while anti-Stokes ones have negative Raman shift (Le Ru & Etchegoin, 2009a). Raman scattering is intrinsically weak since the majority of photons scatter elastically and only one out of 10^6-10^8 photons scatter inelastically (Qin et al., 2019). Raman intensity can be expressed by the following equation (Pelletier, 2003),

$$I = \frac{2^4\pi^3}{45 \cdot 3^2 \cdot c^4} \cdot \frac{hI_L N(v_0 - v)^4}{\mu v(1 - e^{-hv/kT})} [45(\alpha'_a)^2 + 7(\gamma'_a)^2]$$

where c is speed of light, h is Plank's constant, I_L is excitation intensity, N is the number of scattering molecules, v is molecular vibrational frequency in Hertz, v_o is laser excitation, frequency in Hertz, μ is reduced mass of the vibrating atoms, k is Boltzmann constant, T is absolute temperature, α'_a is mean value invariant of the polarizability tensor, and γ'_a is anisotropy invariant of the polarizability tensor. According to the equation, Raman intensity is proportional to the number of scattering molecules. Therefore, Raman spectroscopy can be applied for quantification (Pelletier, 2003).

2.2 Surface-enhanced Raman spectroscopy (SERS)

Surfaced enhanced Raman scattering (SERS) was first discovered through the work of Fleischmann et al, who studied Raman spectra of adsorbed molecules at metal electrode surfaces (Moskovits, 1985). This discovered phenomenon of dramatically enhanced Raman intensities opens the door to identification of trace amounts of substances and even allows single molecule detection (Kneipp et al., 1997). Subsequently, plenty of studies have employed SERS (Sharma et al., 2012) and expanded its applications across many disciplines, including food safety, biosensing, and pharmaceutical analyses (Li & Church, 2014; Yuan et al., 2017; Zheng & He, 2014) Although the explanations for SERS effect are still under debate, electromagnetic and chemical enhancements are widely adopted mechanisms for SERS (Campion & Kambhampati, 1998).

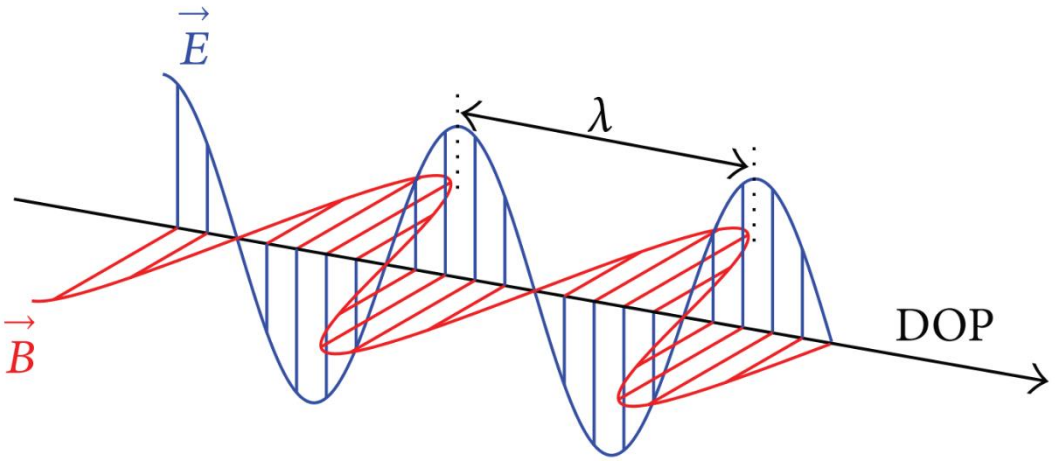

Figure 2.2. Illustration of electromagnetic wave and the directions of propagation (DOP), electric field ($\vec{E}$), and magnetic field ($\vec{B}$) (Vian et al., 2016).

SERS effects derive primarily from the electromagnetic enhancements (Willets & Van Duyne, 2007). Light is a type of electromagnetic wave, and propagation of light generates electric and magnetic fields, which are perpendicular to each other and to the direction of the light flow (Figure 2.2). The magnitudes of both fields fluctuate over time.

When a charged particle, say an electron, moves through the light-generated electric and magnetic fields, it will experience forces of both fields. If light impinges on metallic particles that are smaller than the wavelength of light, it can cause the electron oscillation confined within its structure (Figure 2.3.) (Hammond et al., 2014). The phenomenon of localized oscillation of plasmon is known as localized surface plasmon resonance (LSPR).

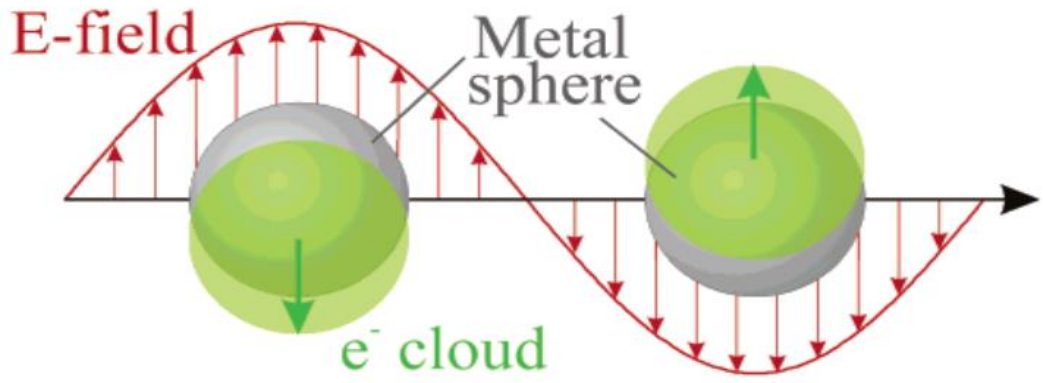

Figure 2.3. Oscillation of electron cloud (Kelly, Coronado, Zhao, & Schatz, 2003).

It is generally regarded that nuclei are static and that electrons can move around. The displacement of electron cloud generates a restoring force that results from Coulomb force between nuclei and electrons (Kelly et al., 2003).

Acceleration of charged particles generate magnetic and electric fields, whose directions and intensities are changing. During a Raman measurement, molecules placed on or close to the metallic nanostructure can experience strong electromagnetic forces resulting from LSPR. These forces are stronger than the forces the molecules would experience without the nanostructure. The regions exposed to the dramatically intensified electromagnetic fields are called “hot spots” (Pilot et al., 2019). LSPR can amplify the surrounding fields and consequently augment Raman scatterings of molecules adsorbed on the surface (Ye et al., 2012). The adsorption can be either physical or chemical. Examples for physisorption include attractive forces such as van der Waals forces, electrostatic forces, and hydrogen

bonding, while chemisorption involves chemical reactions (Le Ru & Etchegoin, 2009b). Several factors influence the frequency of oscillation, including the geometry, size, and materials of the nanostructure.

Although the electromagnetic enhancements are major contribution of SERS effects, chemical enhancements were proposed to complete the explanation for SERS (Le Ru et al., 2007). Chemical enhancements are related to molecular electron configurations and charge transfer between the analyte and metal surface (Wang, Yan, and Chen 2013).

2.3 Gold nanostars

2.3.1 Gold metal

Gold is a noble metal that is not easily oxidized at normal atmospheric pressure and can interact with visible and near infrared lights to generate plasmon resonance (Figure 2.4) (Ghosh & Pal, 2007). Like other noble metals, gold has electrons in conduction band, which can move around easily and hence be readily polarized (Burda et al., 2005). Due to these properties, gold is one of the most used materials for SERS substrates.

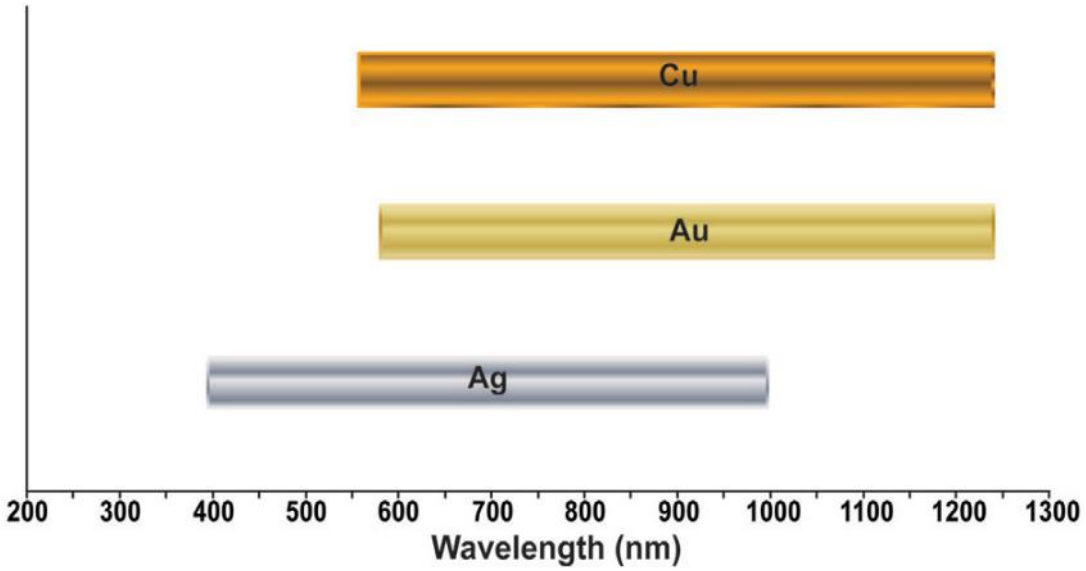

Figure 2.4. Approximate resonance wavelength ranges for copper, gold, and silver (Sharma et al., 2012).

2.3.2 Morphology

Since Raman enhancement is fundamental for SERS phenomena, SERS substrates are utilized for the purpose of enhancing Raman signals from the samples. Magnitudes of enhancements rely heavily on nanostructures of SERS substrates. Plasmon resonance can be localized if the particle size is smaller than the wavelength of light. Nanoparticles are defined as having at least one dimension that is smaller than 100 nm, even if they are part of a larger material or suspending in a medium (Jana et al., 2016). Thus, the collision between nanoparticles and photons of visible and near infrared light can generate LSPR. Additionally, nanoparticles have larger surface areas and are more active than their bulk materials (Burda et al., 2005). Owing to these reasons, a myriad of studies focus on the fabrication of different nanostructures of SERS substrates (Quester et al., 2013; Tiwari et al., 2007).

Among various morphologies, nanostars have attracted great attention. Having plasmon absorption located at near infrared (NIR) region makes gold nanostars desirable for biological research such as tissue imaging and pharmaceutics since tissues do not have strong absorbance in this region (Gobin et al., 2007). Another advantage is that gold nanostars can be excited by NIR lasers, which reduce Rayleigh scattering and risks of melting gold nanoparticles (Suzuki et al., 2004). Furthermore, the spiky tips of gold nanostars can serve as SERS hot spots, which increase the local fields (Guerrero-Martínez et al., 2011; Kleinman et al., 2013). Therefore, analyte molecules adsorbed at hot spots experience intensified electromagnetic forces. The "tip effect" is also known as "lightning rod effect" (Boyack & Le Ru, 2009). The protrusions of nanostars also contribute to considerably large surface area, enabling superior interaction and effective adsorption with analyte molecules (Issaad et al., 2017; Kumari & Singh, 2012). Previous research concluded that nanostsars possess better Raman performance than nanospheres (Nalbant Esenturk & Hight Walker, 2009; Rodríguez-Lorenzo et al., 2009). Hence, nanostar-based SERS substrates have great potential for SERS applications in varied areas.

2.3.3 Fabrication of gold nanostars

Gold nanostars employed in this study were fabricated through a seed mediated method, involving nucleation and crystal growth (Sun et al., 2019). Two moderate reducing agents—citrate and hydroquinone—are chosen to avoid direct reduction of Au^{III} to Au^{0}. Simplistically, the entire process is to reduce Au^{III} to Au^{I} by citrate and subsequently reduce Au^{I} to Au^{0} by hydroquinone (Figure 2.5) (Li et al., 2011). Hydroquinone plays a paramount

role in nanostar synthesis since it selectively reacts with Au^{I} and allows anisotropic growth, leading to formation of outward conical-shaped protrusions.

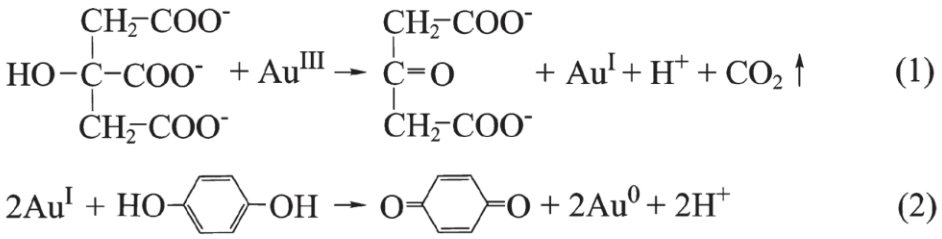

Figure 2.5. The chemical process of gold ion reduction (Li et al., 2011).

CHAPTER 3

MATERIALS AND METHODS

3.1 Materials and chemicals

Gold(III) chloride solution (30 wt. % in dilute HCl), hydroquinone, R6G, TBZ, and paraquat were purchased from Sigma-Aldrich (St. Louis, MO, USA). Sodium citrate dihydrate and acetone were obtained from Fisher Scientific (Fair Lawn, NJ, USA). Apple juice and green tea were brought from a local grocery store. Whatman branded 0.2 μm polyethersulfone (PES) membrane filter devices were used for sample preparation.

3.2 Synthesis of gold nanostars

Gold nanostars were synthesized based on the method of Sun *et al* (Sun, Yu, & Lin, 2019). The synthesis of gold nanostars requires preparation of gold seeds. Briefly, 30 mL of water was heated to boiling and mixed with 300 μL of 1% gold chloride solution with constant stirring, followed by adding 100 ml of 0.1% of sodium citrate dihydrate solution. The mixture was heated and stirred continuously until the color changed to red wine color. To synthesize gold nanostars, 25 μL of 100 mM of gold chloride solution, 50 μL of seed solution, 22 μL of 1% sodium citrate dihydrate solution, and 1 mL of 30 mM hydroquinone solution were added sequentially to 10 mL of water with constant stirring. The mixed solution was stirred at room temperature for 30 min to obtain gold nanostars. To concentrate the gold nanostar solution, the solution was centrifuged, and the supernatant was discarded.

3.3 UV-Visible spectroscopy

A Cary 50 Bio UV–Visible spectrophotometer (Varian, Inc., USA) was used to measure the absorbance of gold seed solution.

3.4 Morphology and element analyses

Prior to the analyses, a volume of 5 μL of gold nanostar solution was dropped and dried on a copper grid. A twin transmission electron microscope (TEM) (FEI Tecnai F30) coupled with an energy dispersive X-ray spectrometer was used to view the shapes and analyze element composition of gold nanostar. A scanning electron microscope (SEM) (Quanta 600 FEG; FEI Company, USA) were used to observe surface morphology of the gold nanostars. The SEM images were taken at 30 kV.

3.5 Zeta potential

Zeta potential of gold nanostars was determined by using Zetasizer Nano ZS (Malvern Instruments Ltd., Worcestershire, UK).

3.6 Preparation of different concentrations of R6G standard solutions

Different concentrations (0, 0.25, 0.5, 1, and 5 ppm) of R6G standard solutions were prepared and water was use as the solvent.

3.7 Preparation of different concentrations of TBZ standard solutions

Different concentrations (0, 0.05, 0.5, 5, 10, 25, and 50 ppm) of TBZ standard solutions were prepared and acetone was use as the solvent.

3.8 Preparation of TBZ in apple juice

Apple juice was filtered through the membrane filter and spiked with TBZ to make different concentrations of TBZ samples (0, 5, 10, 25, and 50 ppm).

3.9 Preparation of different concentrations of paraquat standard solutions

Different concentrations (0, 0.02, 0.2, 5, 10, 25, and 50 ppm) of paraquat standard solutions were prepared and water was use as the solvent.

3.10 Preparation of paraquat in green tea

Green tea was filtered through the membrane filter and spiked with paraquat to make different concentrations of paraquat samples (0, 0.2, 5, 10, 25, and 50 ppm).

3.11 SERS measurements

SERS measurements were conducted by using a DXR2 Raman spectrometer (Thermo Fisher Scientific Inc., USA) with 785 nm laser source. The laser beam (~20 mW laser power) was focus through a 10X objective lens. Raman spectra were collected through

OMNIC software (Thermo Fisher Scientific Inc., Waltham, MA, USA) and Raman measurements were taken from different locations of the samples with 10 scans per measurement and 1 second of exposure time per scan. Ten measurements were averaged for each concentration of the samples. The SERS samples were prepared by dropping 2 μL of gold nanostar suspension onto a slide and mixing with 2 μL of the sample solution. The mixed droplet was dried on a 45°C hot plate prior to the Raman measurements. R6G is a standard SERS probe molecule and was used in this study to evaluate the SERS performance of gold nanostars.

3.12 Raman spectral data analysis

Delight software (Delight, D-squared Development Inc., LaGrande, OR, USA) was utilized for Raman spectral analyses. Spectral data were processed by smoothing and second derivative transformations to decrease noises and increase spectral resolution. The partial least squares (PLS) models were established for prediction of concentrations. The correlation coefficient, R, was used to evaluate how well the PLS model predicts concentrations of the samples. R ranges from 0 to 1. R close to 1 denotes strong positive linear relationship. Root mean squared error of prediction (RMSEP) is a common measure of prediction error for a statistical modeling and is calculated through the following equation,

$$RMSEP = \sqrt{\frac{\sum(y_i - \hat{y})^2}{n}}$$

where y_i is the actual concentration, $\hat{y}$ is the predicted concentration generated by the model, and n is the number of the samples. Ratio of performance to deviation (RPD) value is a ratio of sample standard deviation to the prediction error. The smaller the prediction error the greater the RPD. Thus, higher RPD value signifies better prediction model. Higher R and RPD and lower RMSEP suggest stronger predictive ability of the model. Recovery percentages were calculated by the equation below.

$$Recovery\% = \frac{predictied\ concentraion}{spiked\ concentraion} \times 100\%$$

Limits of detection (LODs) of this SERS method were determined by the student's t test ($p < 0.05$).

CHAPTER 4

RESULTS AND DISCUSSIONS

4.1 Characterization

Figure 4.1A shows the ruby red color of seed solution for gold nanostars; the red color is the result of reflecting red light and absorbing green light. Bulk gold has gold color. Nonetheless, a gold particle can display a different color as the particle size and shape change. An absorption peak located around 520 nm in the UV-vis spectrum of the seed solution indicates the plasmon resonance frequency of gold seed particles (Figure 4.1B) (Ghosh & Pal, 2007). The maximum absorbance peak of seed solution can serve as a quick check for accuracy of synthesis of seed solution.

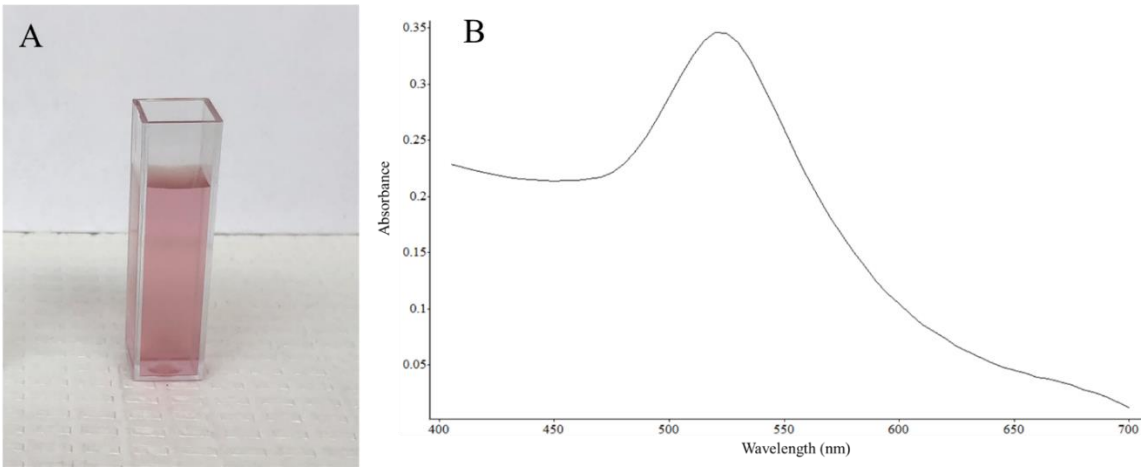

Figure 4.1. The seed solution for gold nanostar (A) and an UV-vis spectrum of the seed solution (B).

Different from the gold seed solution, the gold nanostar solution has blue color and a deep blue color can be seen in its concentrated solution (Figure 4.2). Hydroquinone in growth solution allows increases in the diameters of gold seed nanoparticles and causes the nanoparticles to form multiple outward radiating spikes (Li et al., 2011).

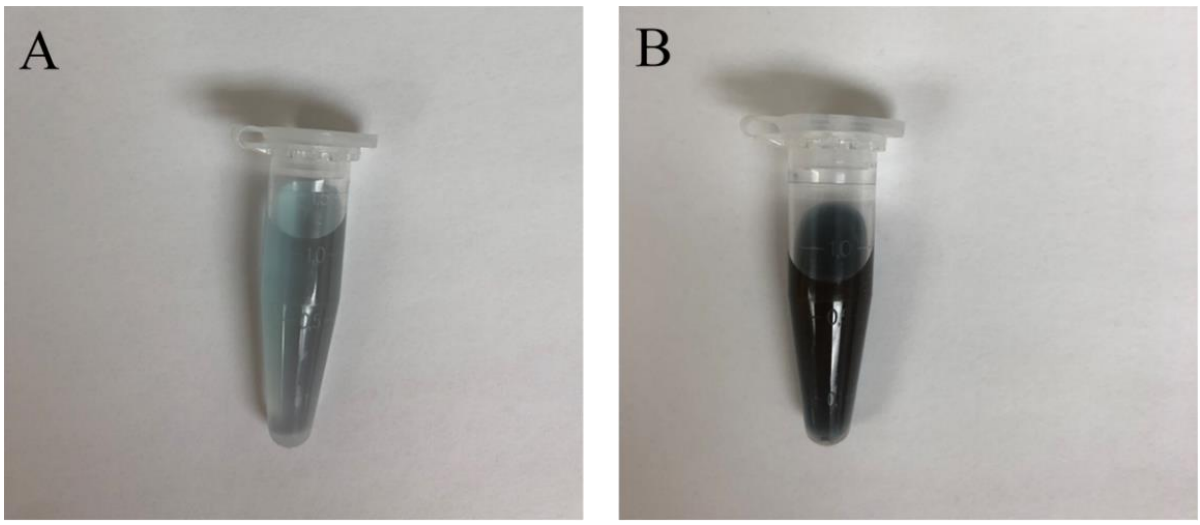

Figure 4.2. The gold nanostar solution (A) and concentrated gold nanostar solution (B).

Figure 4.3 and 4.5 clearly demonstrate the spiky structure and rugged topography of gold nanostars. Compared to smooth surfaces, the rough surfaces of gold nanostars are beneficial to adsorption of analyte molecules because of increased surface areas. It can also be observed that the gold nanostars are homogenous in size and shape. Figure 4.3B and 4.4 show that gold nanostars are composed of gold element. The average diameter, branch width, and branch height of gold nanostars are 248, 47, and 45 nm, respectively (Table 1). The areas around branch tips are where electromagnetic enhancements take place (Khoury & Vo-Dinh, 2008). The average Zeta potential of gold nanostars is -29.53; the high absolute value of zeta potential means that the colloidal suspension of gold nanostars has high stability.

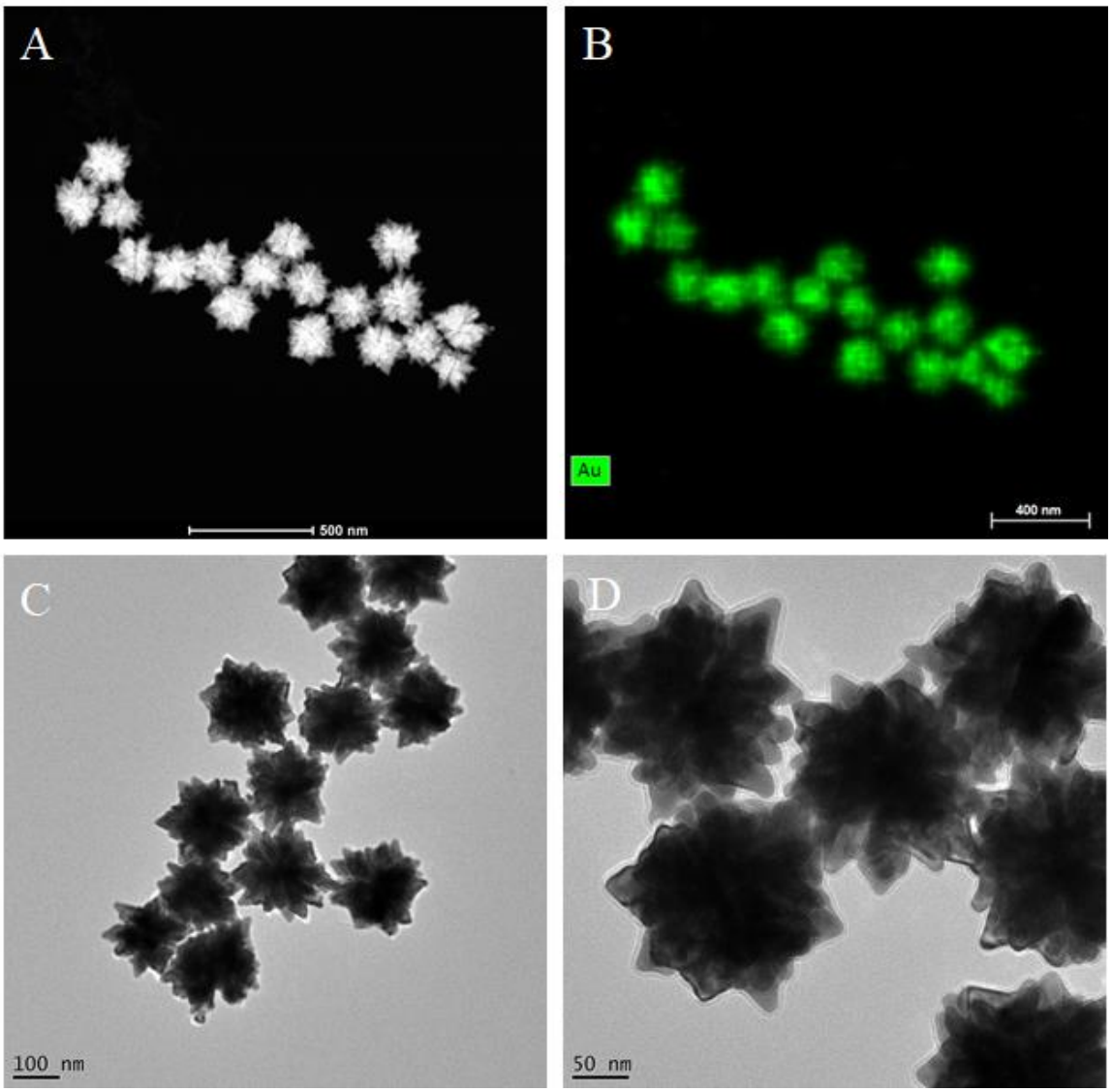

Figure 4.3. A STEM image of gold nanostars (A) and its corresponding EDS image (B); TEM images of gold nanostars with 100 nm and 50 nm scale bars, respectively (C and D).

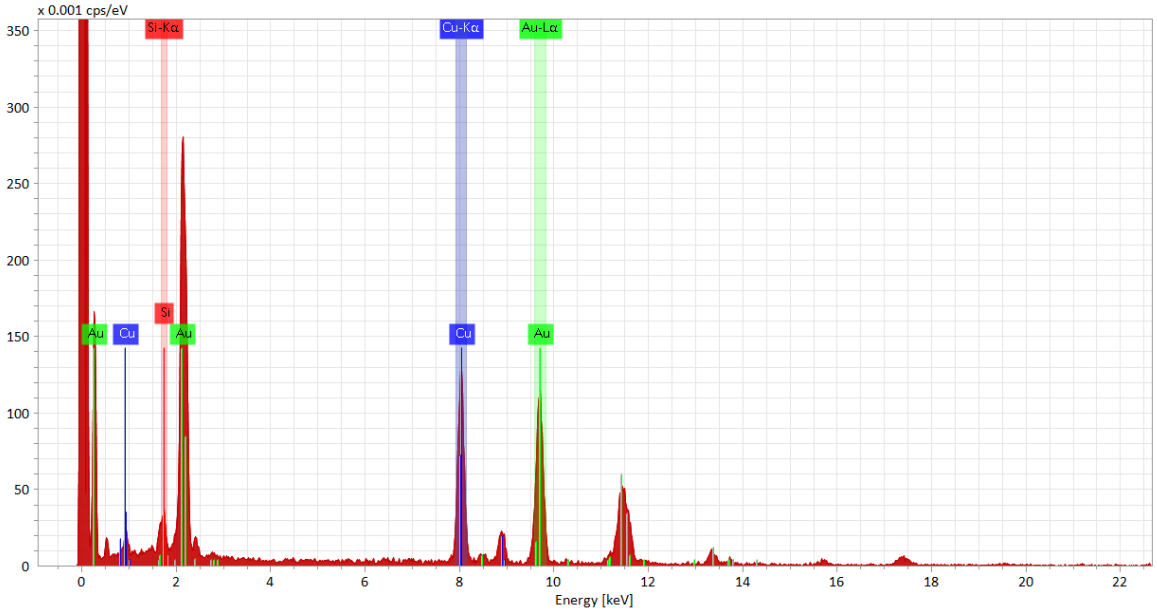

Figure 4.4. An EDS spectrum of gold nanostars. (note the copper comes from TEM grip and the silicon comes from the EDS detector.)

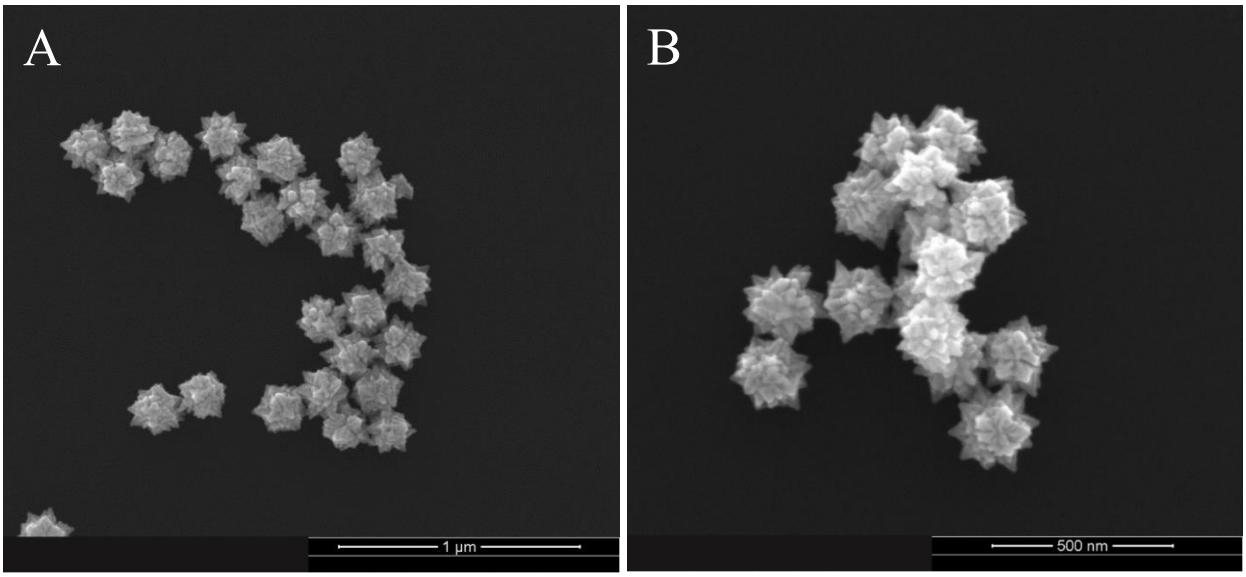

Figure 4.5. SEM images of gold nanostars at different scales.

Table 1. Measurements of gold nanostars.

	Branch width	Branch height	Diameter
Measurement (nm)	47 ± 3.6	45 ± 5.8	248 ± 8.1

Each value is expressed as mean ± standard deviation (SD) (n = 10)

4.2 Evaluation of SERS performance of gold nanostars

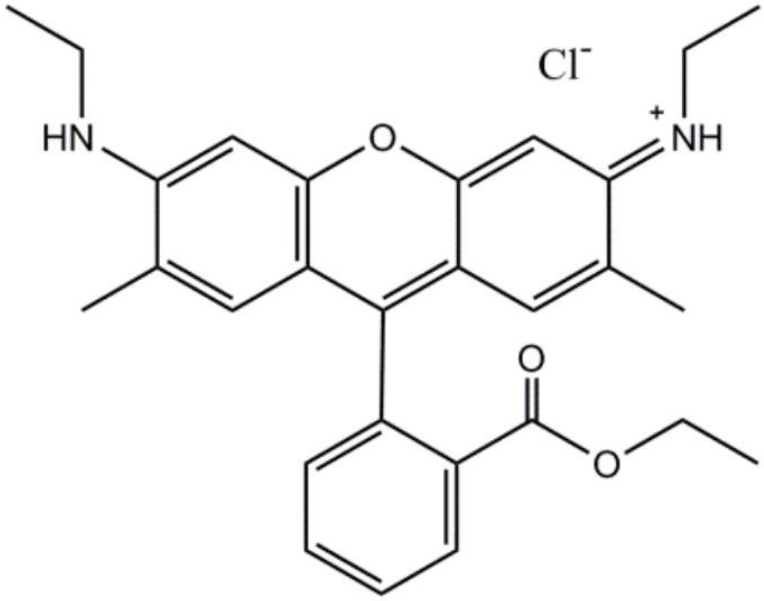

Figure 4.6. Chemical structure of R6G (Wu et al. 2019).

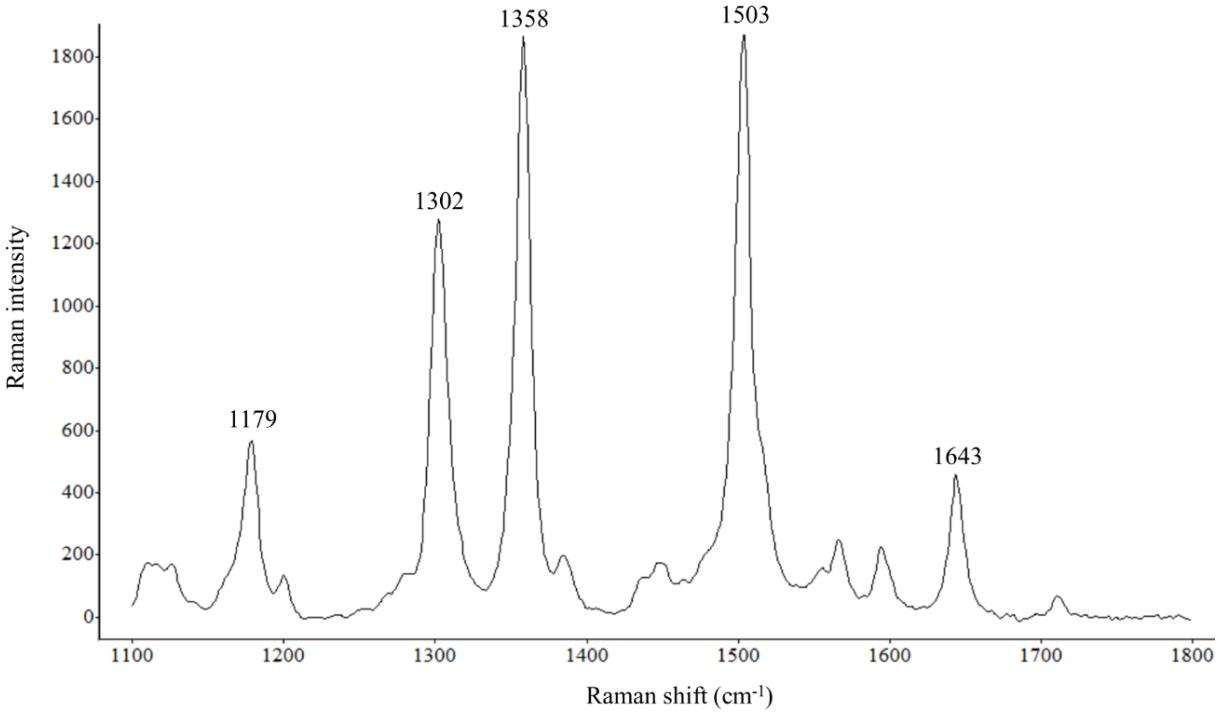

Figure 4.7. A Raman spectrum of R6G powder.

SERS activity of as-prepared gold nanostar substrate was assessed by measuring different concentrations of R6G. R6G is commonly used Raman probe and a dye belonging to xanthene family. As illustrated in Figure 4.6, R6G is composed of a xanthene core and a phenyl ring. Figure 4.7 exhibits a representative Raman spectrum of R6G powder, showing three very strong peaks appear at 1302, 1358, and 1503 cm^{-1} and two medium strong peaks at 1179 and 1643 cm^{-1}. These peaks are due to vibrations of xanthene ring (Mullin & Schatz, 2012; Wu et al., 2019).

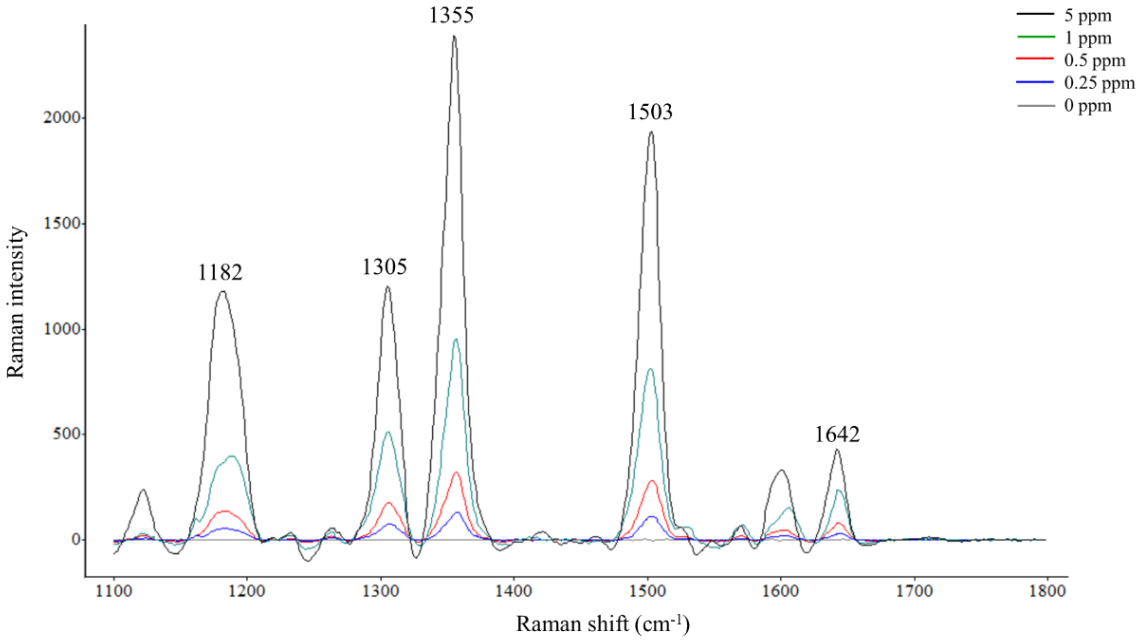

Figure 4.8. SERS spectra of different concentrations of R6G solutions.

Figure 4.8 shows the SERS spectra of different concentrations of R6G solutions. The characteristic peaks located at 1182, 1305, 1355, 1503, and 1642 cm^{-1} can be easily seen. The positions of these peaks only slightly shift compared to those of the major peaks shown in the Raman spectrum of R6G powder. The intensities of the peaks increase as the concentration of R6G solutions increase. The distinct peaks can still be observed at 0.25 ppm of R6G, suggesting the gold nanostars is a good and sensitive SERS substrate.

4.3 Determination of TBZ in solution

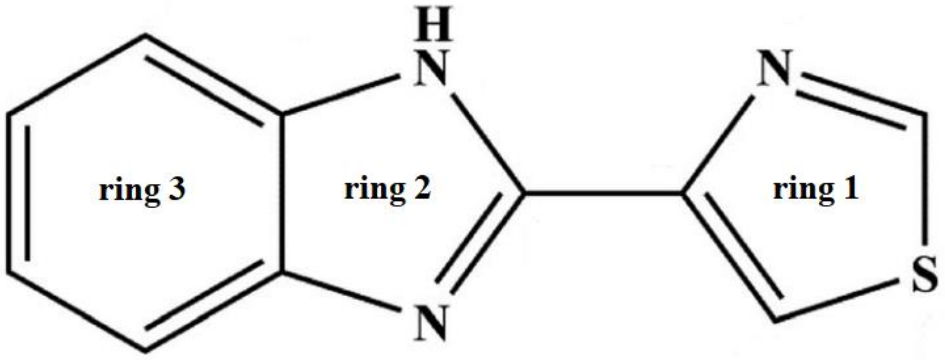

Figure 4.9. Chemical structure of TBZ (Sun et al., 2018).

Table 2. Raman peak assignments for TBZ (Feng, Hu, Grant, & Lu, 2018; Luo, Huang, Lai, Rasco, & Fan, 2016; Muller, David, Chis, & Pinzaru, 2014)

Pesticide	Peak (cm^{-1})	Assignments
TBZ	780	υ(S-C) ring 1, δ(C=N) ring 1, δ(C-N) ring 1, and δ(C-C) ring 3
	1012	υ(C-N) ring 2, υ(C-C) ring 2 and 3, δ(N=C-N) ring 2 and 3, δ(C-H) ring 1
	1277	υ(C-C) ring 1, υ(C-N) ring 2, δ(C-C-H) ring 2, δ(C-H) ring 1, δ(C=N-N) ring 2
	1455	δ(C-H) ring 1
	1578	υ(C-C) ring 2, υ(C=N) ring 2, υ(C=C) ring 3, υ(C-C) ring 3, δ(C-H) ring 2, δ(C-N-H) ring 2.

Note: υ = stretching, δ = bending.

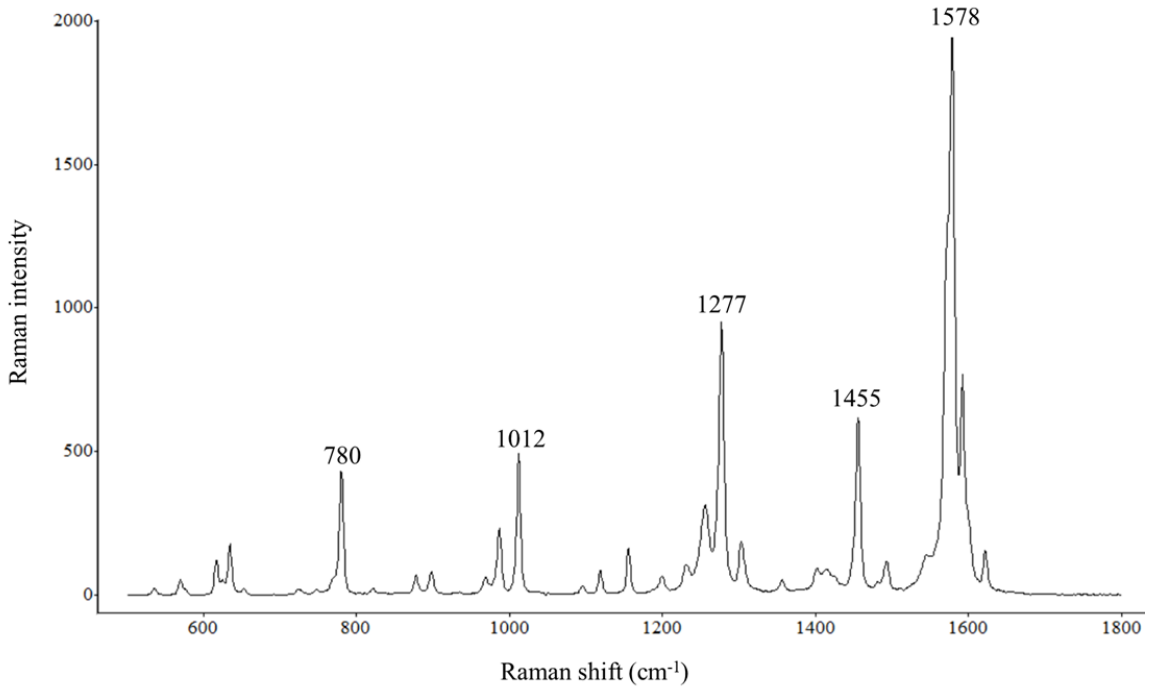

Figure 4.10. A Raman spectrum of TBZ powder.

TBZ is composed of three aromatic rings as depicted in Figure 4.9. The pi electrons in the rings, sulfur, and nitrogen can be adsorbed on gold surfaces (Kim et al., 2009). Raman spectra of TBZ powder were measured to investigate characteristic peaks of TBZ. Figure 4.10 conveys the dominant peaks of TBZ at 780, 1012, 1277, 1455, and 1578 cm^{-1}. The peak assignments are listed in Table 2 (Feng et al., 2018; Luo et al., 2016; Muller et al., 2014). The peak at 780 cm^{-1} is assigned to S-C stretching in ring 1, C=N bending in ring 1, C-N bending in ring 1, and C-C bending in ring 3. The appearance of peak at 1012 cm^{-1} is attributed to C-N stretching in ring 2, C-C stretching in ring 2 and 3, N=C-N bending in ring 2 and 3, and C-H bending in ring 1. The peak present at 1578 cm^{-1} is the contribution of multiple vibrations including C-C stretching in ring 2, C=N stretching in ring 2, C=C

stretching in ring 3, C-C stretching in ring 3, C-H bending in ring 2, and C-N-H bending in ring 2.

Figure 4.11A displays the SERS spectra of different concentrations of TBZ solutions (0, 0.05, 0.5, 5, 10, 25, and 50 ppm). The major peaks in the SERS spectra of TBZ in solution are located at 785, 1012, 1276, and 1596 cm^{-1}, which are similar to the positions of those primary peaks in the Raman spectrum of TBZ powder. The increasing trend of peak intensities as the TBZ concentration increases can be noticed from the spectra. Derivative transformations are commonly applied to eliminate baseline shift and improve discrimination. The second derivative SERS spectra of TBZ in solution shows the intensities are concentration-dependent (Figure 4.11B).

Figure 4.12A shows the PLS model based on the spectral data acquired from different concentrations of TBZ. The model can be used for prediction of TBZ concentration in the solution. The R value and RMSEP are 0.9754 and 3.921, respectively. A good linear relationship between actual concentrations and predicted concentrations can be concluded by the R value, which is close to 1. The loading plot indicates that peaks at around 785, 1012, and 1596 cm^{-1} are the major contributions to the PLS model (Figure 4.12B). The RPD is greater than 3, conveying that the PLS model is good (Table 3). The recovery% is 89.4% and the limit of detection is 0.05 ppm. These results suggest that gold nanostar substrate is promising in quantification of TBZ.

Table 3. The PLS results and LOD for TBZ in solution.

Sample	RPD	Recovery (%)	LOD (ppm)
TBZ standard solution	4.427	89.4%	0.05

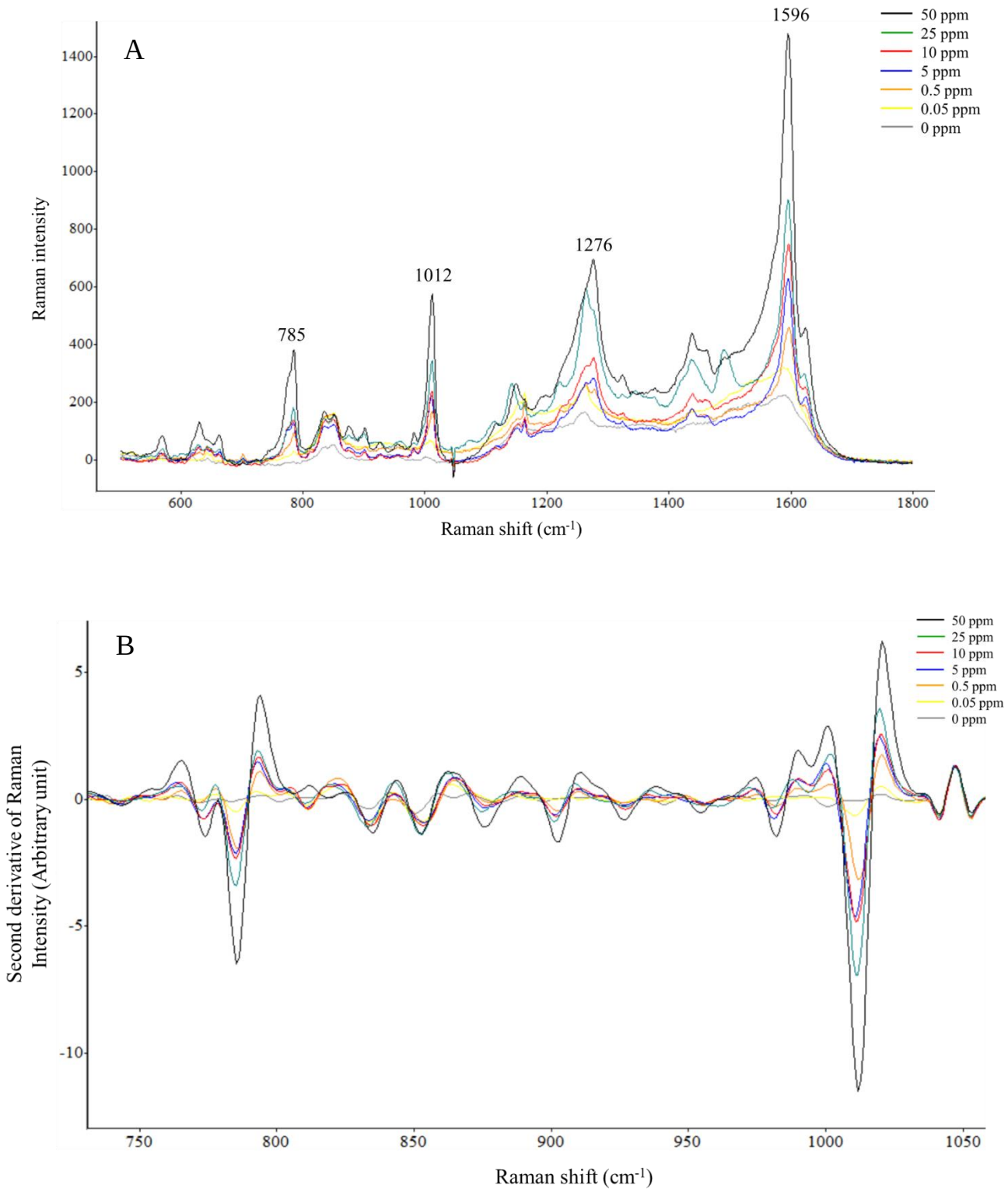

Figure 4.11. SERS spectra of different concentrations of TBZ solutions (A); second derivative SERS spectra of TBZ solutions (B).

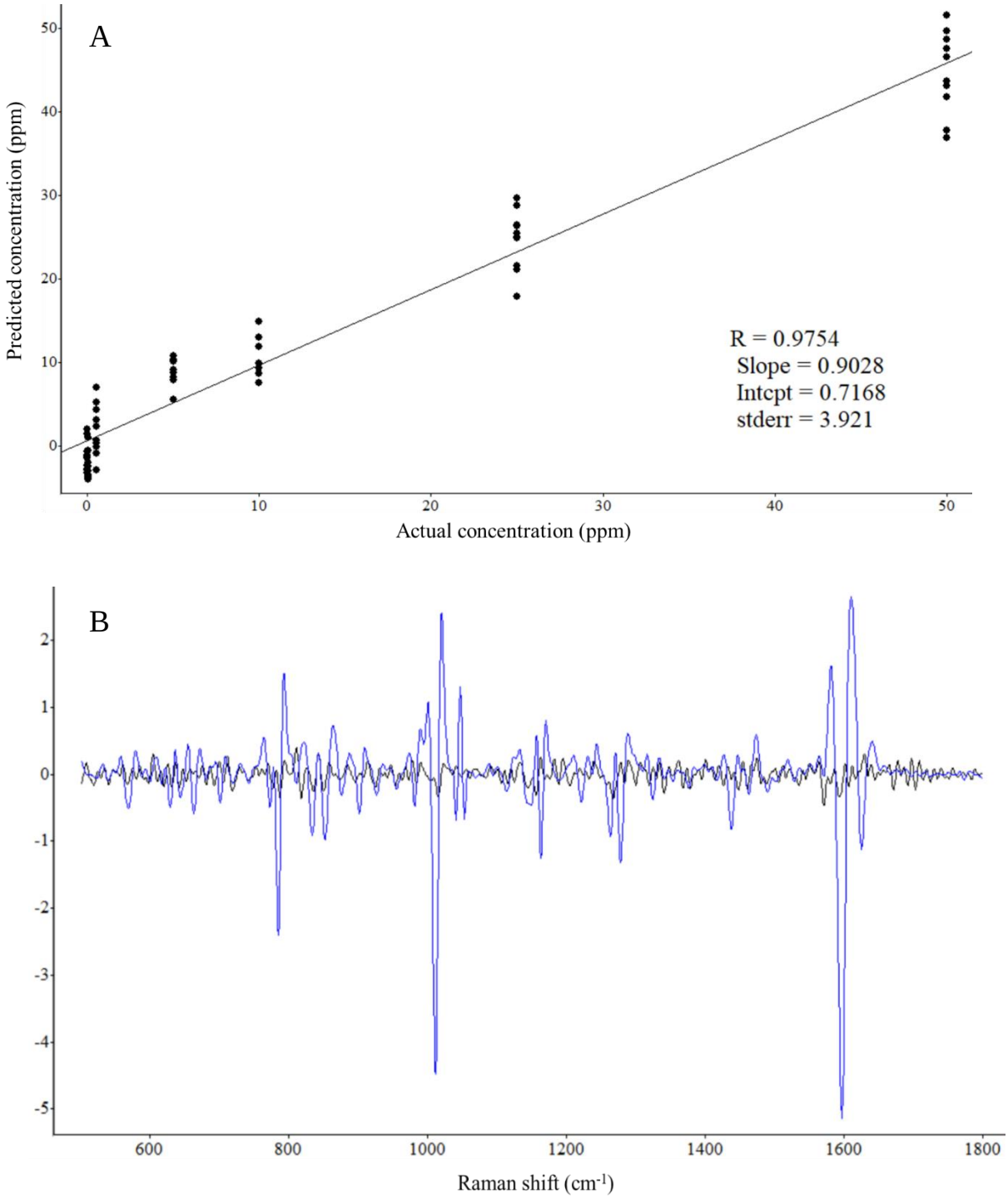

Figure 4.12. Prediction of TBZ concentration in solution using the PLS model (A); the loading plot of PLS model (B).

4.4 Determination of TBZ in apple juice

Apples are considered “Dirty” fruits due to their high potential of contamination with pesticide residues and have been classified as high-pesticide residue food based on pesticide residue burden score (PRBS), which is derived from data collected by United States Department of Agriculture (USDA) (Wesselink et al., 2020; Winter & Katz, 2011). Pesticides can be defined as systematic or non-systematic. Systematic pesticides like TBZ can permeate plant tissues and be found in the pulp and juice (Albero et al., 2005). Therefore, apple juice was chosen as the food matrix for this study to simulate trace TBZ detection in a real food sample.

SERS spectra of various concentrations of TBZ in apple juice are exhibited in Figure 4.13A. The characteristic peaks of TBZ can be identified at 783, 1008, 1266, and 1594 cm^{-1}, which are consistent with dominant peaks of TBZ present in SERS spectra of TBZ powder. The intensities decline as the TBZ concentrations decrease. The second derivative spectra of TBZ in apple juice also demonstrate a similar pattern as the TBZ levels reduced (Figure 4.13B).

One of the great challenges of SERS application for trace analyses in food samples is the complexity of food components such as carbohydrates, proteins, phytochemicals, etc. These components can hinder the detection in several ways. Some substances within foods are Raman active and can make analyte identification difficult (Qu et al., 2020). Large molecules such as proteins and some carbohydrates can reduce the number of hot spots by

causing spatial segregation among nano-entities of SERS substrates. The comparatively immense structures of large molecules can also wrap around nanostructure of SERS substrates and analytes, hence obstructing substrate-analyte interactions (Stosch et al., 2005). In addition, apple juices contain sugars such as sucrose, glucose, and fructose, which can significantly lower Raman intensities of analyte molecules (Luo et al., 2018). Since SERS effects are also influenced by the surroundings, acids and overall food matrix can make the environment unfavorable for Raman enhancements (Dou et al., 1999). Nevertheless, the characteristic peaks of TBZ are still discernible at 5 ppm level of TBZ in apple juice.

PLS analysis for quantification of TBZ in apple juice is shown in Figure 4.14A. The R value and RMSEP are 0.9657 and 4.798, respectively. The loading plot of PLS model shows that the peaks at 783, 1008, 1594 cm^{-1} are important for the modeling (Figure 4.14B). The RPD value implies the PLS model is satisfactory (Table 5). The recovery is 92.3%, and the limit of detection is less than MRL (12 ppm) for apple pomace set by the United State environmental protection agency (EPA).

Table 4. The PLS results and LOD for TBZ in apple juice.

Sample	RPD	Recovery (%)	LOD (ppm)
TBZ in apple juice	3.801	92.3%	5

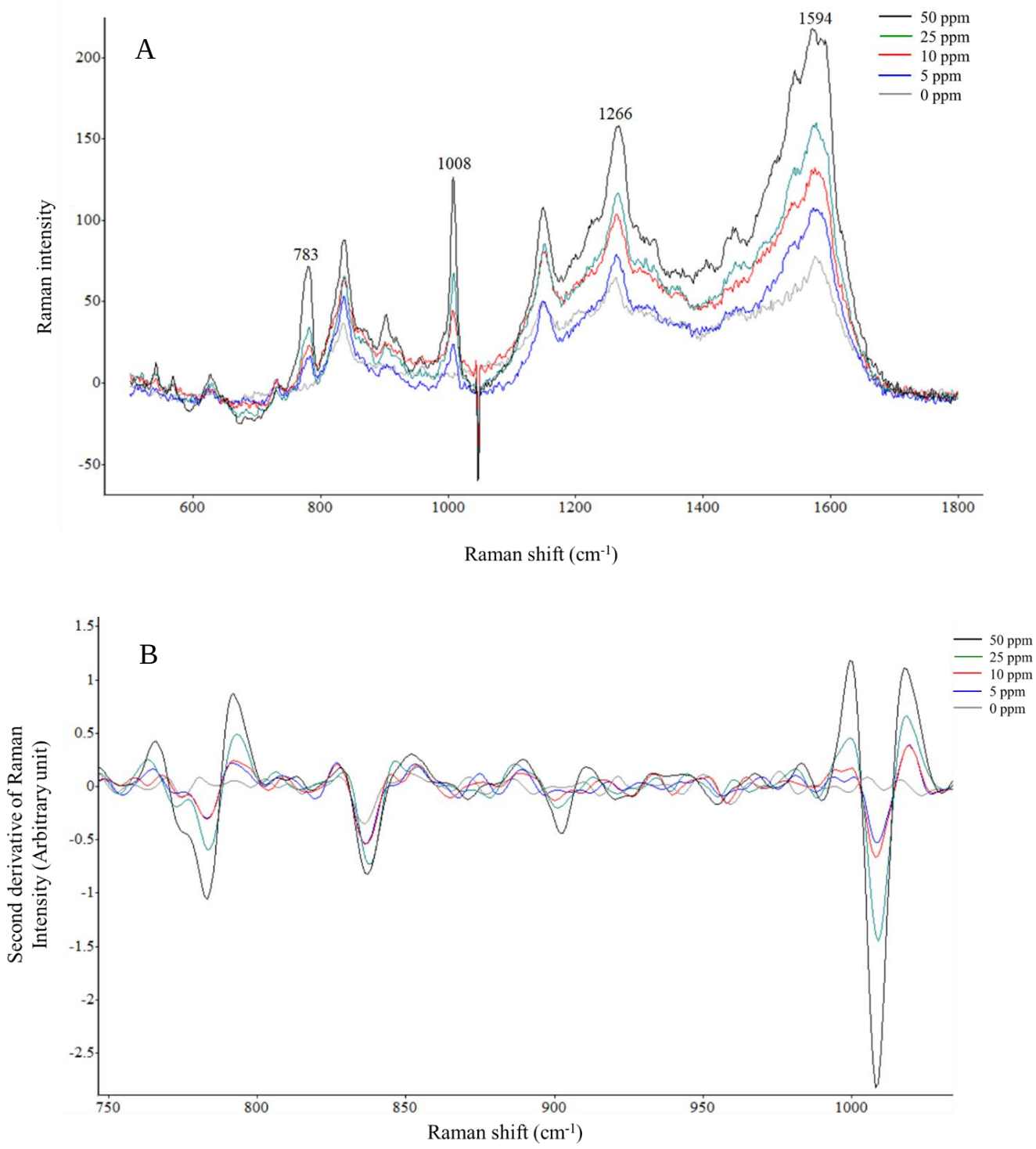

Figure 4.13 SERS spectra of different concentrations of TBZ in apple juice (A); second derivative SERS spectra of TBZ in apple juice (B).

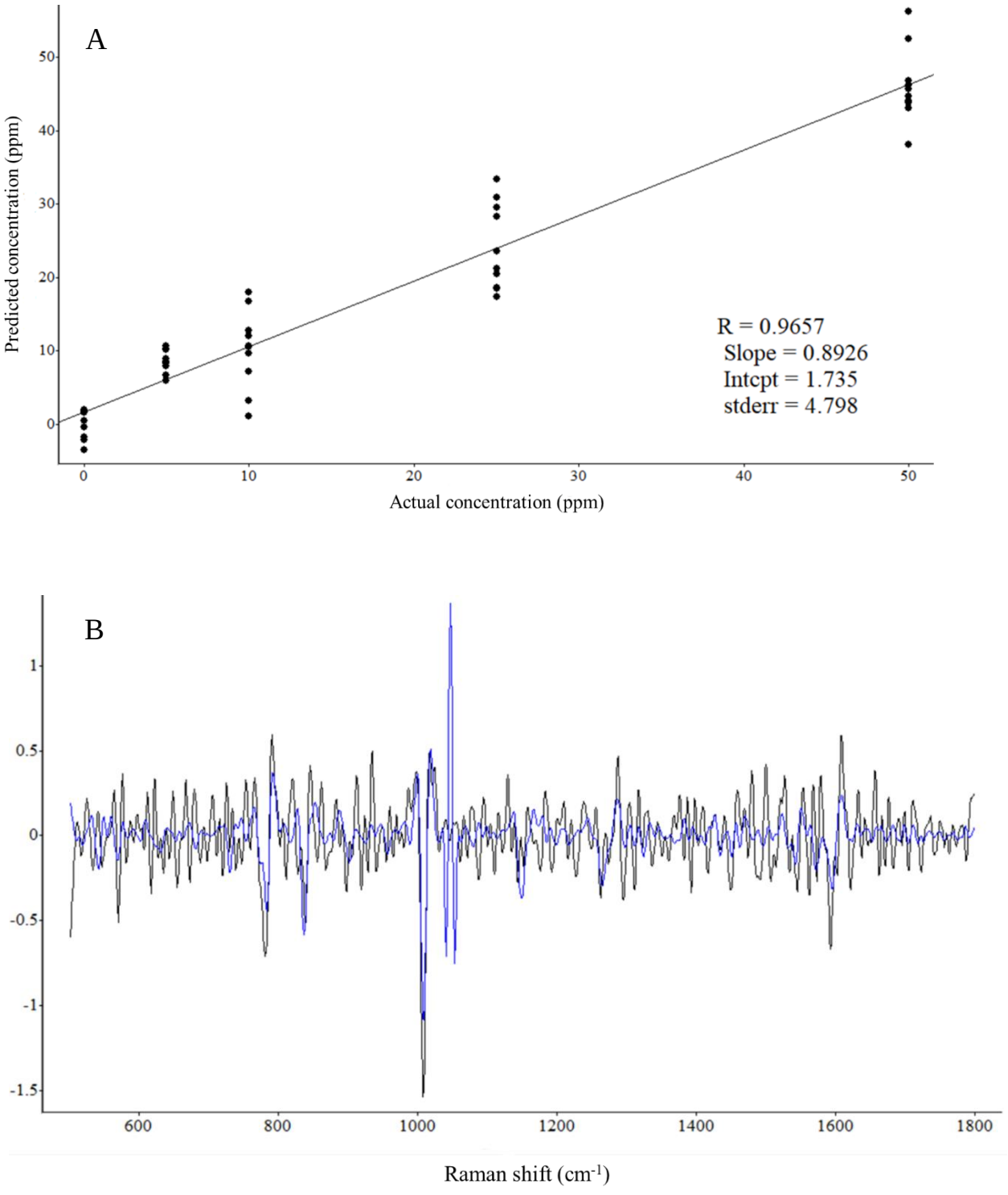

Figure 4.14. Prediction of TBZ concentration in apple juice using the PLS model (A) and the corresponding loading plot of PLS model (B).

4.5 Determination of paraquat in solution

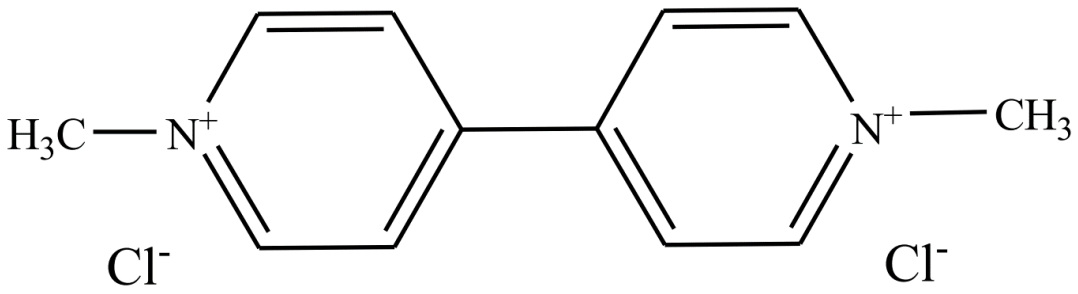

Figure 4.15. Chemical structure of paraquat (Insuwan & Rangsriwatananon, 2017).

Table 5. Raman peak assignments for paraquat (Tsen et al., 2019).

Pesticide	Peak (cm^{-1})	Assignments
Paraquat	839	υ(C-N)
	1198	δ(C=C)
	1298	C-C structural distortion
	1653	υ(C=N)

Note: υ = stretching, δ = bending.

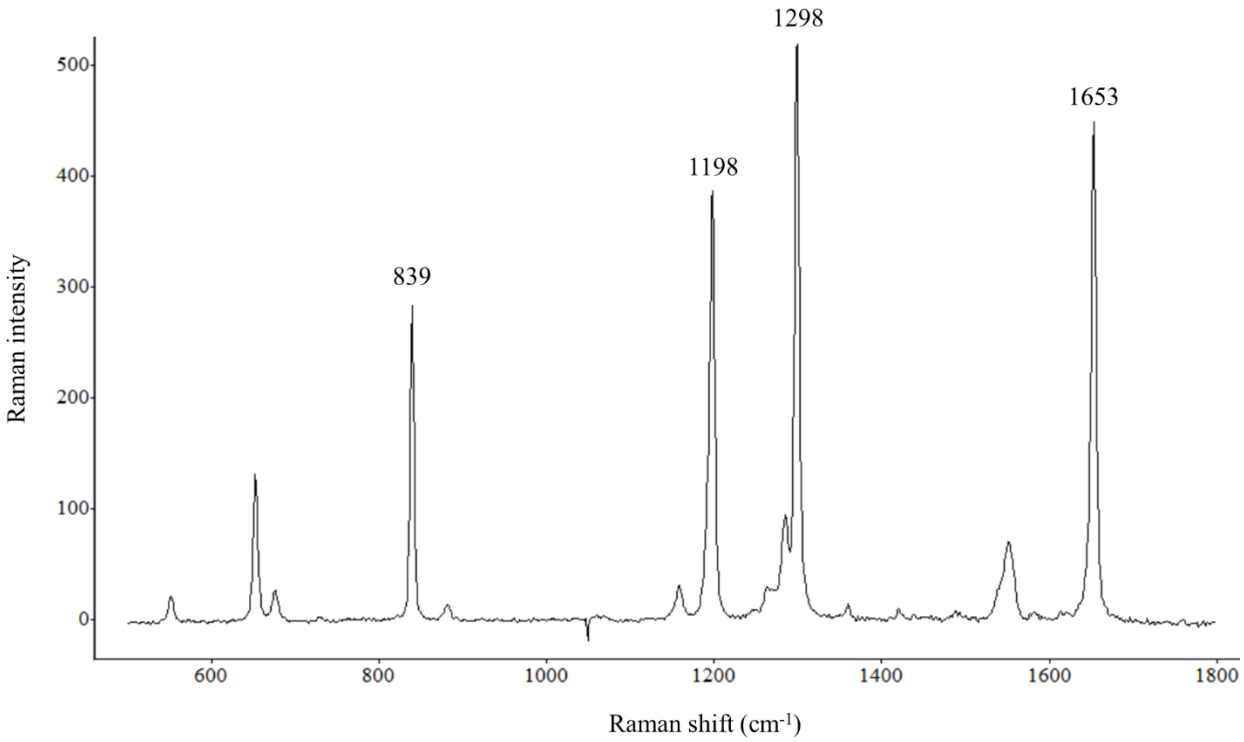

Figure 4.16. A Raman spectrum of paraquat powder.

Paraquat (1,1' dimethyl-4,4'-bipyridynium dichloride) refers to a kind of quats, which are quaternary ammonium compounds. They are permanently positively charged regardless of the pH value in the solution and usually contain anions in their chemical formula (Shackman et al., 2015). As presented in Figure 4.15, paraquat consists of C-N, C=N, C-C, C=C, and C-H bonds. The representative Raman spectrum of paraquat powder clearly demonstrates the characteristic peaks of paraquat (Figure 4.16). These peaks are located at 839, 1198, 1298, and 1653 cm^{-1} and ascribed to C-N stretching, C=N bending, C-C structural distortion, and C=N stretching, respectively (Table 5).

Figure 4.17A shows the SERS spectra of different concentrations of paraquat in the aqueous solutions. The principal SERS peaks for paraquat appear at 836, 1184, 1290, 1637 cm^{-1}, and the strongest peak positions at 1637 cm^{-1}. These results are in accordance with other study (Botta et al., 2020). In addition, higher concentrations of paraquat result in higher Raman signals and the second derivative spectra also reveal the tendency of increased intensities as the paraquat concentrations increase. The PLS model built upon the SERS spectra of paraquat standard solutions has the RMSEP equivalent to 1.693 (Figure 4. 18A). The strong linearity between actual and predicted values is evidenced by a high R value of 0.9953. The loading plot conveys that the pronounced peaks of paraquat are the most influential factors for the modeling (Figure 4.18B). The RPD value is greater than 10, meaning the PLS model is robust (Table 6). The recovery is 99.6% and limit of detection is 0.02 ppm. These results signify that the gold nanostars is a promising SERS substrate for quantification of paraquat.

Table 6. The PLS results and LOD for paraquat in solution.

Sample	RPD	Recovery (%)	LOD (ppm)
Paraquat standard solution	10.27	99.6%	0.02

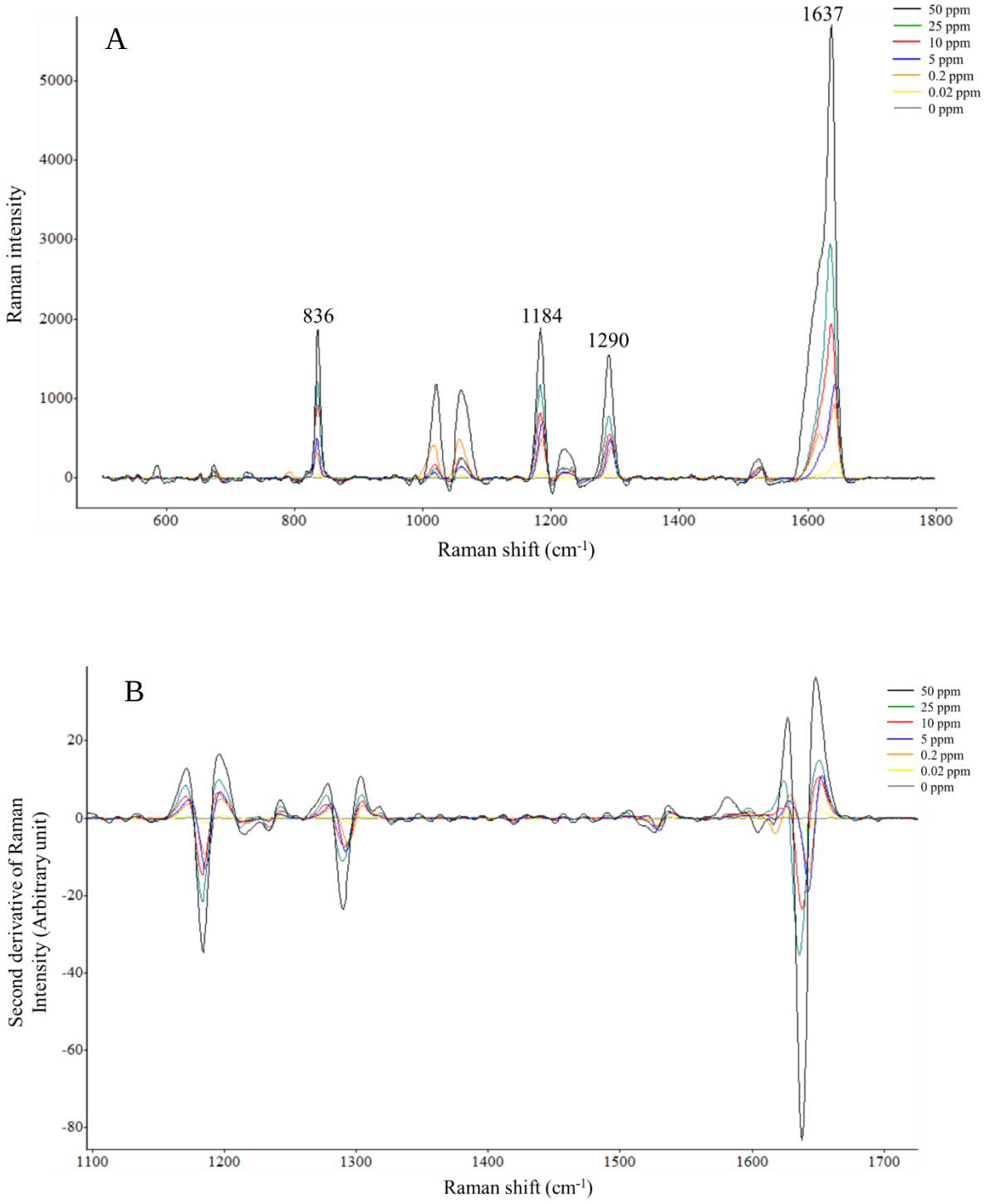

Figure 4.17. SERS spectra of different concentrations of paraquat solutions (A); second derivative SERS spectra of paraquat solutions (B).

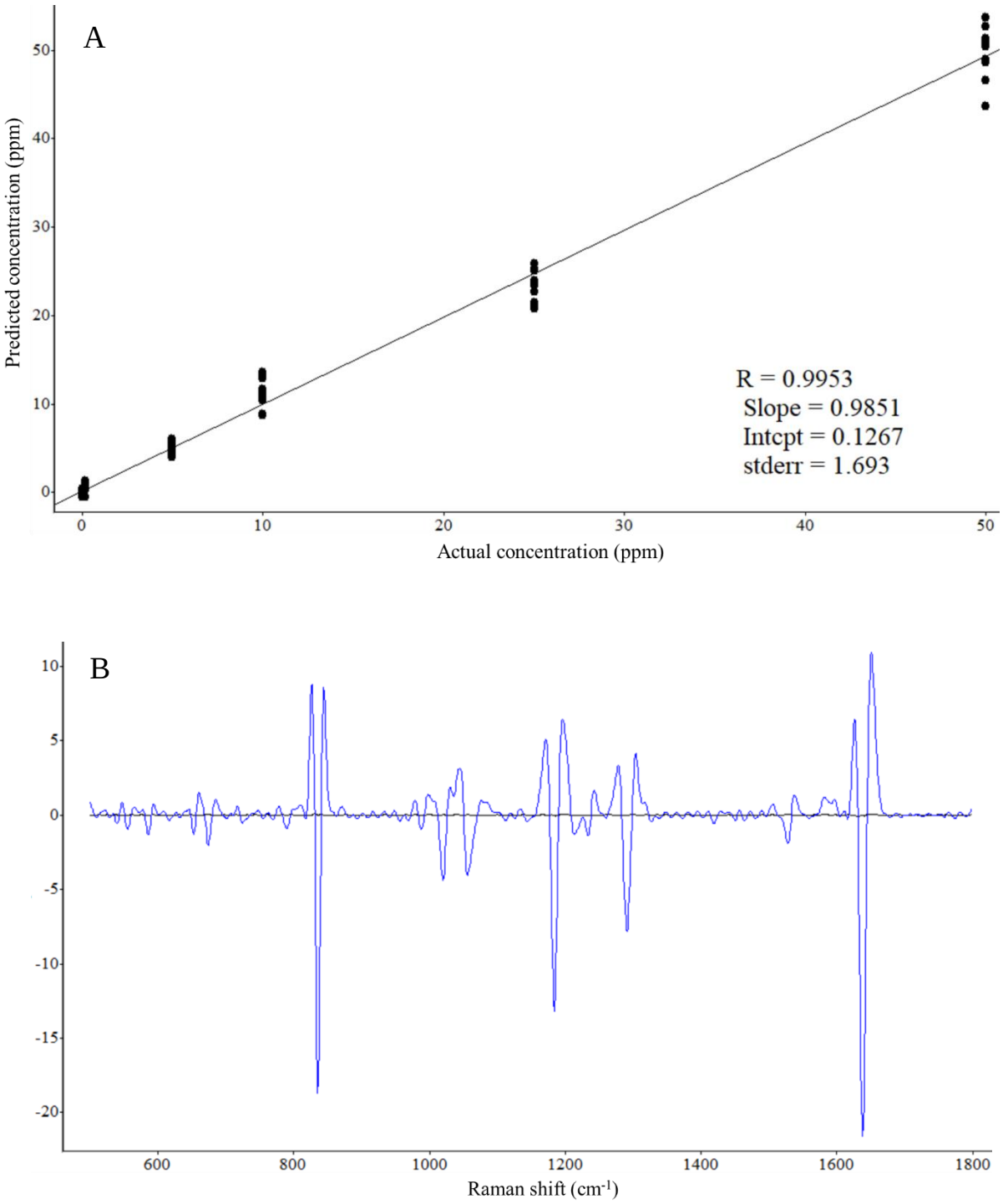

Figure 4.18. Prediction of paraquat concentration in solution using the PLS model (A) and the corresponding loading plot of PLS model (B).

4.6 Determination of paraquat in green tea

Tea is one of the most popular beverages and an important global agricultural commodity. Black tea, green tea, and oolong tea are three widely consumed tea. The oxidation degree is the determining factor for distinguishing these three types of teas. Black tea is fully oxidized while green tea is little oxidized, and oolong tea is in the middle of black and green tea. Due to the least degree of processing, green tea retains more polyphenols than the other two. It also contains tannin, caffeine, volatile oils, and some B vitamins (Hicks, 2009).

Pesticides are crucial for raising agricultural products including tea. The 2018 European Union report conducted by European Food Safety Authority (EFSA) states that more than 15% of the sampled teas contain pesticide residues above the corresponding MRLs (EFSA, 2020). Paraquat, a nonselective pesticide, can be applied to tea cultivation for weed control. The MRL of paraquat for tea is 0.2 ppm according to CODEX, which is an international guideline and a foundation for many countries' regulations. In this study, green tea was intentionally added with different amounts of paraquat and gold nanostars were used as a SERS substrate to evaluate the SERS performance of gold nanostars in the real food samples.

Figure 4.19 present SERS spectra and the second derivative transformations of different concentrations of paraquat in the green tea. The characteristic peaks of paraquat can be clearly seen at 834, 1184, 1292, and 1640 cm^{-1}, which are only slightly shifted compared

to the peaks of SERS spectra of paraquat powder. Other compounds within the green tea such as polyphenols and caffeine do not significantly interfere the identification of paraquat, and the primary peaks of paraquat are still discernable at 0.2 ppm level of paraquat. Moreover, the positive relationship between the paraquat concentrations and Raman intensities can be noted from the spectra. The PLS model and loading plot are illustrated in Figure 4.20. The R and RMSEP values are 0.99 and 2.524, respectively. The high R value denotes a strong linear correlation between the actual and predicted concentrations. The loading plot is similar to the loading plot of paraquat standard solution and indicates the characteristic peaks of paraquat are the main contributors to the modeling. The RPD suggest the adequacy of the PLS model (Table 7). The recovery is 100.1% and the limit of detection of paraquat in green tea is 0.2 ppm, equivalent to the CODEX standard.

Table 7. The PLS results and LOD for paraquat in green tea.

Sample	RPD	Recovery (%)	LOD (ppm)
Paraquat in green tea	7.098	100.1%	0.2

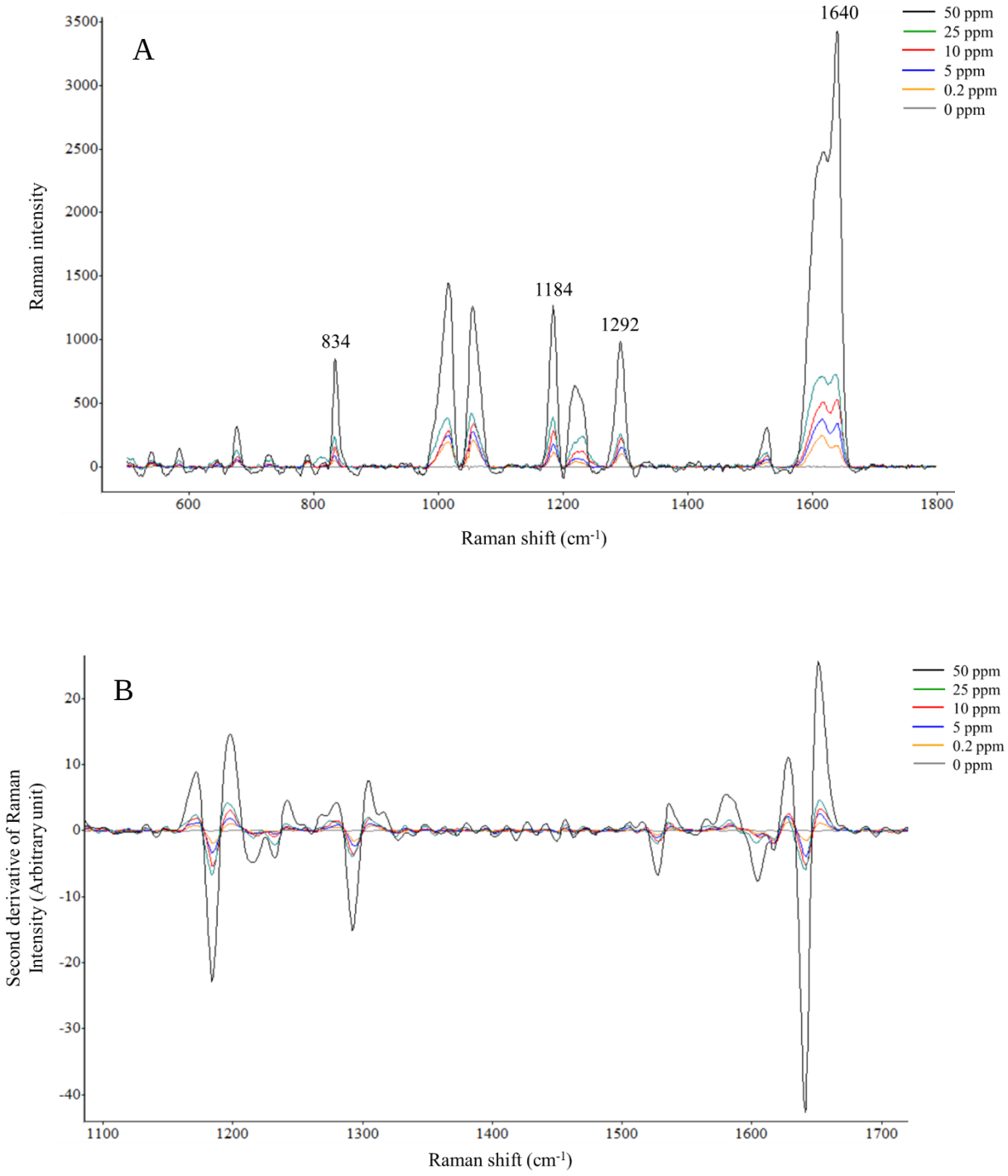

Figure 4.19. SERS spectra of different concentrations of paraquat in green tea (A); second derivative SERS spectra of paraquat in green tea (B).

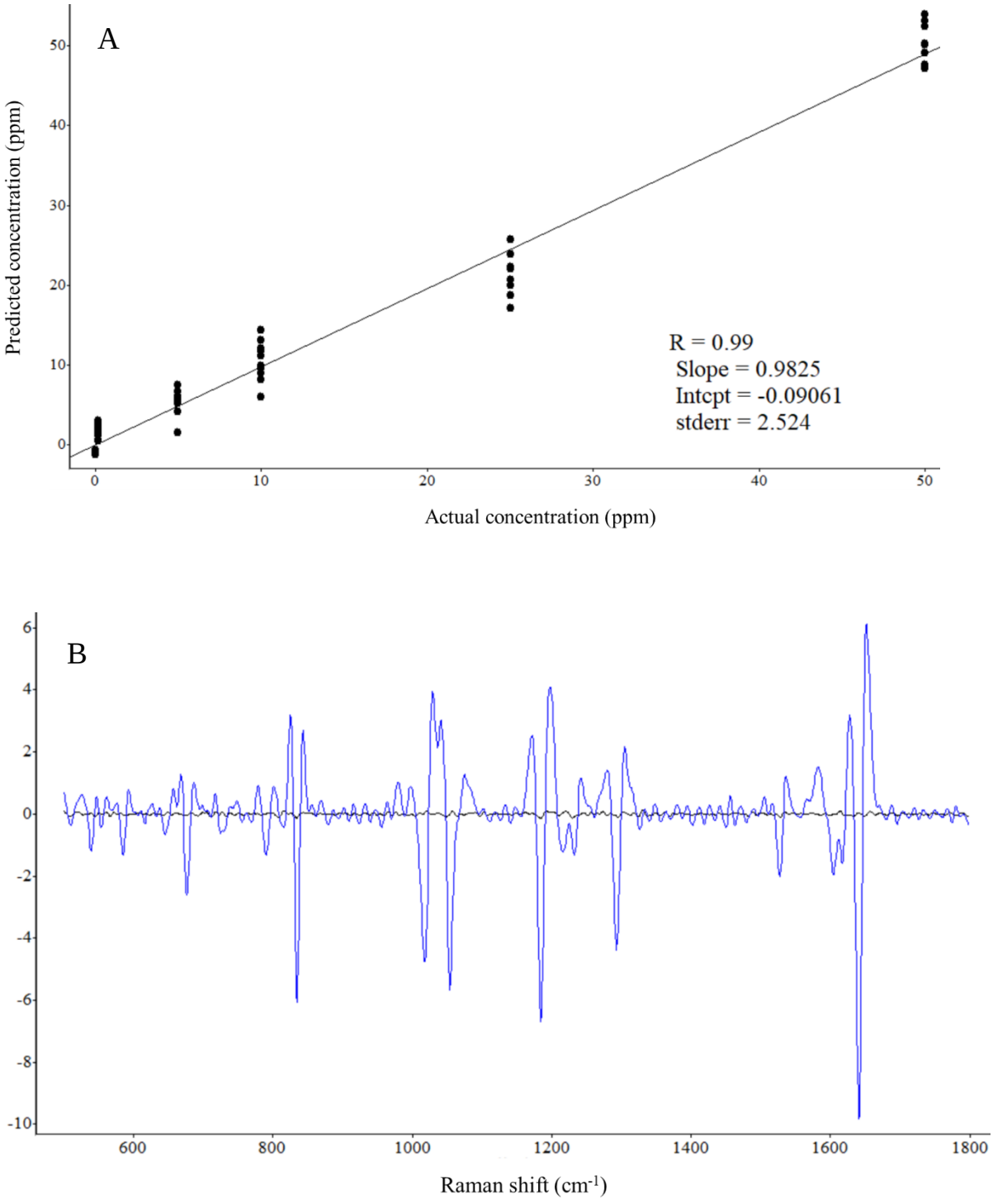

Figure 4.20. Prediction of paraquat concentration in green tea using the PLS model (A) and the corresponding loading plot of PLS model (B).

CHAPTER 5

CONCLUSIONS AND FUTURE STUDIES

SERS is a rising and alternative detection technique. In this study, SERS performance of a novel SERS substrate, gold nanostars, was evaluated by detecting two different pesticides in the real food samples. Zetasizer and the electron microscopes were used for characterization of the substrate. The detection limits are 5 ppm for TBZ in apple juice and 0.2 ppm for paraquat in green tea. The satisfactory results conclude that this SERS method is rapid and effective and has great potential to be applied for qualification and quantification of food contaminants. Nevertheless, there is still some room to optimize SERS performance. Future studies can focus on developing approaches to orderly arrange the gold nanostars and improving sample preparation to reach even lower detection limits.

REFERENCES

Ahmad, A., Shahid, M., Khalid, S., Zaffar, H., Naqvi, T., Pervez, A., Bilal, M., Ali, M. A., Abbas, G., & Nasim, W. (2019). Residues of endosulfan in cotton growing area of vehari, pakistan: An assessment of knowledge and awareness of pesticide use and health risks. *Environmental Science and Pollution Research*, *26*(20), 20079-20091. https://doi.org/10.1007/s11356-018-3169-6

Albero, B., Sánchez-Brunete, C., & Tadeo, J. L. (2005). Multiresidue determination of pesticides in juice by solid-phase extraction and gas chromatography–mass spectrometry. *Talanta*, *66*(4), 917-924. https://doi.org/https://doi.org/10.1016/j.talanta.2004.12.046

Allen, P. M., & Gottlieb, D. (1970). Mechanism of action of the fungicide thiabendazole, 2-(4'-thiazolyl) benzimidazole. *Applied Microbiology*, *20*(6), 919-926. https://doi.org/doi:10.1128/aem.20.6.919-926.1970

Alvarez-Puebla, R., Liz-Marzán, L. M., & García de Abajo, F. J. (2010). Light concentration at the nanometer scale. *The Journal of Physical Chemistry Letters*, *1*(16), 2428-2434. https://doi.org/10.1021/jz100820m

Bala, R., Dhingra, S., Kumar, M., Bansal, K., Mittal, S., Sharma, R. K., & Wangoo, N. (2017). Detection of organophosphorus pesticide – malathion in environmental samples using peptide and aptamer based nanoprobes. *Chemical Engineering Journal*, *311*, 111-116. https://doi.org/https://doi.org/10.1016/j.cej.2016.11.070

Bhandari, G., Zomer, P., Atreya, K., Mol, H. G. J., Yang, X., & Geissen, V. (2019). Pesticide residues in nepalese vegetables and potential health risks. *Environmental Research*, *172*, 511-521. https://doi.org/https://doi.org/10.1016/j.envres.2019.03.002

Boatemaa, S., Barney, M., Drimie, S., Harper, J., Korsten, L., & Pereira, L. (2019). Awakening from the listeriosis crisis: Food safety challenges, practices and governance in the food retail sector in south africa. *Food Control*, *104*, 333-342. https://doi.org/https://doi.org/10.1016/j.foodcont.2019.05.009

Botta, R., Eiamchai, P., Horprathum, M., Limwichean, S., Chananonnawathorn, C., Patthanasettakul, V., Maezono, R., Jomphoak, A., & Nuntawong, N. (2020). 3D structured laser engraves decorated with gold nanoparticle sers chips for paraquat herbicide detection in environments. *Sensors and Actuators B: Chemical*, *304*, 127327. https://doi.org/https://doi.org/10.1016/j.snb.2019.127327

Boyack, R., & Le Ru, E. C. (2009). Investigation of particle shape and size effects in SERS using t-matrix calculations [10.1039/B905645A]. *Physical Chemistry Chemical Physics*, *11*(34), 7398-7405. https://doi.org/10.1039/B905645A

Burda, C., Chen, X., Narayanan, R., & El-Sayed, M. A. (2005). Chemistry and properties of nanocrystals of different shapes. *Chemical Reviews*, *105*(4), 1025-1102. https://doi.org/10.1021/cr030063a

Campion, A., & Kambhampati, P. (1998). Surface-enhanced Raman scattering [10.1039/A827241Z]. *Chemical Society Reviews*, *27*(4), 241-250. https://doi.org/10.1039/A827241Z

Cognet, L., & Lounis, B. (2008). Ultra-sensitive detection of individual gold nanoparticles: Spectroscopy and applications to biology. *Gold Bulletin*, *41*(2), 139-146. https://doi.org/10.1007/BF03216591

Djekic, I., Jankovic, D., & Rajkovic, A. (2017). Analysis of foreign bodies present in European food using data from rapid alert system for food and feed (rasff). *Food Control*, *79*, 143-149. https://doi.org/https://doi.org/10.1016/j.foodcont.2017.03.047

Donkor, A., Osei-Fosu, P., Dubey, B., Kingsford-Adaboh, R., Ziwu, C., & Asante, I. (2016). Pesticide residues in fruits and vegetables in ghana: A review. *Environmental science and pollution research 23*(19), 18966-18987. https://doi.org/10.1007/s11356-016-7317-6

Dou, X., Jung, Y. M., Cao, Z.-Q., & Ozaki, Y. (1999). Surface-enhanced Raman scattering of biological molecules on metal colloid ii: Effects of aggregation of gold colloid and comparison of effects of ph of glycine solutions between gold and silver colloids. *Applied Spectroscopy*, *53*(11), 1440-1447. https://doi.org/10.1366/0003702991945803

European Food Safety Authority, Medina-Pastor, P., & Triacchini, G. (2020). The 2018 European Union report on pesticide residues in food. *EFSA Journal*, *18*(4), 6057, 6103 pp. https://doi.org/10.2903/j.efsa.2020.6057

Ember, K. J. I., Hoeve, M. A., McAughtrie, S. L., Bergholt, M. S., Dwyer, B. J., Stevens, M. M., Faulds, K., Forbes, S. J., & Campbell, C. J. (2017). Raman spectroscopy and regenerative medicine: A review. *NPJ Regenerative medicine*, *2*, 12. https://doi.org/10.1038/s41536-017-0014-3

Feng, J., Hu, Y., Grant, E., & Lu, X. (2018). Determination of thiabendazole in orange juice using an MISPE-SERS chemosensor. *Food Chemistry*, *239*, 816-822. https://doi.org/https://doi.org/10.1016/j.foodchem.2017.07.014

Frederix, F., Friedt, J.-M., Choi, K.-H., Laureyn, W., Campitelli, A., Mondelaers, D., Maes, G., & Borghs, G. (2003). Biosensing based on light absorption of nanoscaled gold and silver particles. *Analytical Chemistry*, *75*(24), 6894-6900. https://doi.org/10.1021/ac0346609

Frimpong, J. O., Ofori, E. S. K., Yeboah, S., Marri, D., Offei, B. K., Apaatah, F., Sintim, J. O., Ofori-Ayeh, E., & Osae, M. (2018). Evaluating the impact of synthetic herbicides on soil dwelling macrobes and the physical state of soil in an agro-ecosystem. *Ecotoxicology and Environmental Safety*, *156*, 205-215. https://doi.org/https://doi.org/10.1016/j.ecoenv.2018.03.034

Gawarammana, I. B., & Buckley, N. A. (2011). Medical management of paraquat ingestion. *British Journal of Clinical Pharmacology*, *72*(5), 745-757. https://doi.org/10.1111/j.1365-2125.2011.04026.x

Ghosh, P. K., Debu, D. T., French, D. A., & Herzog, J. B. (2017). Calculated thickness dependent plasmonic properties of gold nanobars in the visible to near-infrared light regime. *PloS One*, *12*(5), e0177463-e0177463. https://doi.org/10.1371/journal.pone.0177463

Ghosh, S. K., & Pal, T. (2007). Interparticle coupling effect on the surface plasmon resonance of gold nanoparticles: From theory to applications. *Chemical Reviews*, *107*(11), 4797-4862. https://doi.org/10.1021/cr0680282

Gobin, A. M., Lee, M. H., Halas, N. J., James, W. D., Drezek, R. A., & West, J. L. (2007). Near-infrared resonant nanoshells for combined optical imaging and photothermal cancer therapy. *Nano Letters*, *7*(7), 1929-1934. https://doi.org/10.1021/nl070610y

Guerrero-Martínez, A., Barbosa, S., Pastoriza-Santos, I., & Liz-Marzán, L. M. (2011). Nanostars shine bright for you: Colloidal synthesis, properties and applications of branched metallic nanoparticles. *Current Opinion in Colloid & Interface Science*, *16*(2), 118-127. https://doi.org/https://doi.org/10.1016/j.cocis.2010.12.007

Hammond, J. L., Bhalla, N., Rafiee, S. D., & Estrela, P. (2014). Localized surface plasmon resonance as a biosensing platform for developing countries. *Biosensors (Basel)*, *4*(2), 172-188. https://doi.org/10.3390/bios4020172

Hicks, A. (2009). Current status and future development of global tea production and tea products. *Assumption University of Journal of Technology*, *12*, 251-264.

Hongmei, L., Xiaxia, Y., Ningning, G., Jun, T., Xiaoyi, L., & Junwei, H. (2020). Microwave method synthesis of magnetic ionic liquid/gold nanoparticles as ultrasensitive sers substrates for trace clopidol detection. *Analytical and Bioanalytical Chemistry*, *412*(13), 3063-3071. https://doi.org/10.1007/s00216-020-02588-7

Huang, Y., Zhan, H., Bhatt, P., & Chen, S. (2019). Paraquat degradation from contaminated environments: Current achievements and perspectives. *Frontiers in Microbiology*, *10*, 1754-1754. https://doi.org/10.3389/fmicb.2019.01754

Insuwan, W., & Rangsriwatananon, K. (2017). Removal of paraquat from aqueous solutions onto zeolite ltl. *Engineering Journal*, *21*, 15-23. https://doi.org/10.4186/ej.2017.21.2.15

Issaad, D., Moustaoui, H., Medjahed, A., Lalaoui, L., Spadavecchia, J., Bouafia, M., de la Chapelle, M. L., & Djaker, N. (2017). Scattering correlation spectroscopy and Raman spectroscopy of thiophenol on gold nanoparticles: Comparative study between nanospheres and nanourchins. *The Journal of Physical Chemistry C*, *121*(33), 18254-18262. https://doi.org/10.1021/acs.jpcc.7b05355

Jallow, M. F. A., Awadh, D. G., Albaho, M. S., Devi, V. Y., & Thomas, B. M. (2017). Pesticide risk behaviors and factors influencing pesticide use among farmers in kuwait. *Science of the Total Environment*, *574*, 490-498. https://doi.org/https://doi.org/10.1016/j.scitotenv.2016.09.085

Jamieson, J. D., Smith, E. B., Dalvie, D. K., Stevens, G. J., & Yanochko, G. M. (2011). Myeloperoxidase-mediated bioactivation of 5-hydroxythiabendazole: A possible mechanism of thiabendazole toxicity. *Toxicology in Vitro*, *25*(5), 1061-1066. https://doi.org/https://doi.org/10.1016/j.tiv.2011.04.007

Jana, J., Ganguly, M., & Pal, T. (2016). Enlightening surface plasmon resonance effect of metal nanoparticles for practical spectroscopic application [10.1039/C6RA14173K]. *RSC Advances*, *6*(89), 86174-86211. https://doi.org/10.1039/C6RA14173K

Jeanmaire, D. L., & Van Duyne, R. P. (1977). Surface Raman spectroelectrochemistry: Part i. Heterocyclic, aromatic, and aliphatic amines adsorbed on the anodized silver electrode. *Journal of Electroanalytical Chemistry and Interfacial Electrochemistry*, *84*(1), 1-20. https://doi.org/https://doi.org/10.1016/S0022-0728(77)80224-6

Kelly, K. L., Coronado, E., Zhao, L. L., & Schatz, G. C. (2003). The optical properties of metal nanoparticles: The influence of size, shape, and dielectric environment. *The Journal of Physical Chemistry B*, *107*(3), 668-677. https://doi.org/10.1021/jp026731y

Khoury, C. G., & Vo-Dinh, T. (2008). Gold nanostars for surface-enhanced Raman scattering: Synthesis, characterization and optimization. *Journal of Physical Chemistry. C: Nanomaterials and Interfaces*, *2008*(112), 18849-18859. https://doi.org/10.1021/jp8054747

Kim, M.-S., Kim, M.-K., Lee, C.-J., Jung, Y. M., & Lee, M.-S. (2009). Surface-enhanced Raman spectroscopy of benzimidazolic fungicides: Benzimidazole and thiabendazole. *Bulletin of the Korean Chemical Society*, *30*, 2930-2934. https://doi.org/10.5012/bkcs.2009.30.12.2930

Kleinman, S. L., Frontiera, R. R., Henry, A.-I., Dieringer, J. A., & Van Duyne, R. P. (2013). Creating, characterizing, and controlling chemistry with SERS hot spots [10.1039/C2CP42598J]. *Physical Chemistry Chemical Physics*, *15*(1), 21-36. https://doi.org/10.1039/C2CP42598J

Kneipp, K., Wang, Y., Kneipp, H., Perelman, L. T., Itzkan, I., Dasari, R. R., & Feld, M. S. (1997). Single molecule detection using surface-enhanced Raman scattering (SERS). *Physical Review Letters*, *78*(9), 1667-1670. https://doi.org/10.1103/PhysRevLett.78.1667

Kumari, S., & Singh, R. P. (2012). Glycolic acid-g-chitosan-gold nanoflower nanocomposite scaffolds for drug delivery and tissue engineering. *International Journal of Biological Macromolecules*, *50*(3), 878-883. https://doi.org/https://doi.org/10.1016/j.ijbiomac.2011.10.014

Le Ru, E. C., Blackie, E., Meyer, M., & Etchegoin, P. G. (2007). Surface enhanced Raman scattering enhancement factors: A comprehensive study. *The Journal of Physical Chemistry C*, *111*(37), 13794-13803. https://doi.org/10.1021/jp0687908

Le Ru, E. C., & Etchegoin, P. G. (2009a). Chapter 2 - Raman spectroscopy and related optical techniques. In E. C. Le Ru & P. G. Etchegoin (Eds.), *Principles of surface-enhanced raman spectroscopy* (pp. 29-120). Elsevier. https://doi.org/https://doi.org/10.1016/B978-0-444-52779-0.00008-8

Le Ru, E. C., & Etchegoin, P. G. (2009b). Chapter 4 - SERS enhancement factors and related topics. In E. C. Le Ru & P. G. Etchegoin (Eds.), *Principles of surface-enhanced Raman spectroscopy* (pp. 185-264). Elsevier. https://doi.org/https://doi.org/10.1016/B978-0-444-52779-0.00010-6

Li, C., Huang, Y., Lai, K., Rasco, B. A., & Fan, Y. (2016). Analysis of trace methylene blue in fish muscles using ultra-sensitive surface-enhanced Raman spectroscopy. *Food Control*, *65*, 99-105. https://doi.org/https://doi.org/10.1016/j.foodcont.2016.01.017

Li, J., Wu, J., Zhang, X., Liu, Y., Zhou, D., Sun, H., Zhang, H., & Yang, B. (2011). Controllable synthesis of stable urchin-like gold nanoparticles using hydroquinone to tune the reactivity of gold chloride. *The Journal of Physical Chemistry C*, *115*(9), 3630-3637. https://doi.org/10.1021/jp1119074

Li, Y. S., & Church, J. S. (2014). Raman spectroscopy in the analysis of food and pharmaceutical nanomaterials. *Journal of Food and Drug Analysis*, *22*(1), 29-48. https://doi.org/10.1016/j.jfda.2014.01.003

Luo, H., Huang, Y., Lai, K., Rasco, B. A., & Fan, Y. (2016). Surface-enhanced Raman spectroscopy coupled with gold nanoparticles for rapid detection of phosmet and thiabendazole residues in apples. *Food Control*, *68*, 229-235. https://doi.org/https://doi.org/10.1016/j.foodcont.2016.04.003

Luo, H., Wang, X., Huang, Y., Lai, K., Rasco, B. A., & Fan, Y. (2018). Rapid and sensitive surface-enhanced Raman spectroscopy (SERS) method combined with gold nanoparticles for determination of paraquat in apple juice. *Journal of the Science of Food and Agriculture*, *98*(10), 3892-3898. https://doi.org/10.1002/jsfa.8906

Moskovits, M. (1985). Surface-enhanced spectroscopy. *Reviews of Modern Physics*, *57*(3), 783-826. https://doi.org/10.1103/RevModPhys.57.783

Muller, C., David, L., Chis, V., & Pinzaru, S. C. (2014). Detection of thiabendazole applied on citrus fruits and bananas using surface enhanced Raman scattering. *Food Chemistry*, *145*, 814-820. https://doi.org/10.1016/j.foodchem.2013.08.136

Mullin, J., & Schatz, G. C. (2012). Combined linear response quantum mechanics and classical electrodynamics (qm/ed) method for the calculation of surface-enhanced Raman spectra. *The Journal of Physical Chemistry A*, *116*(8), 1931-1938. https://doi.org/10.1021/jp2087829

Nalbant Esenturk, E., & Hight Walker, A. R. (2009). Surface-enhanced Raman scattering spectroscopy via gold nanostars. *Journal of Raman Spectroscopy*, *40*(1), 86-91. https://doi.org/10.1002/jrs.2084

Narenderan, S. T., Meyyanathan, S. N., & Babu, B. (2020). Review of pesticide residue analysis in fruits and vegetables. Pre-treatment, extraction and detection techniques. *Food Research International*, *133*, 109141. https://doi.org/https://doi.org/10.1016/j.foodres.2020.109141

Pelletier, M. J. (2003). Quantitative analysis using Raman spectrometry. *Applied Spectroscopy*, *57*(1), 20a-42a. https://doi.org/10.1366/000370203321165133

Pilot, R., Signorini, R., Durante, C., Orian, L., Bhamidipati, M., & Fabris, L. (2019). A review on surface-enhanced raman scattering. *Biosensors*, *9*(2), 57. https://doi.org/10.3390/bios9020057

Pires, S. M., Majowicz, S., Gill, A., & Devleesschauwer, B. (2019). Global and regional source attribution of shiga toxin-producing escherichia coli infections using analysis of outbreak surveillance data. *Epidemiology and Infection*, *147*, e236-e236. https://doi.org/10.1017/S095026881900116X

Qin, J., Kim, M. S., Chao, K., Dhakal, S., Cho, B.-K., Lohumi, S., Mo, C., Peng, Y., & Huang, M. (2019). Advances in Raman spectroscopy and imaging techniques for quality and safety inspection of horticultural products. *Postharvest Biology and Technology*, *149*, 101-117. https://doi.org/https://doi.org/10.1016/j.postharvbio.2018.11.004

Qu, Y., Tian, Y., Chen, Y., & He, L. (2020). Chemical profiling of red wines using surface-enhanced Raman spectroscopy (sers) [10.1039/D0AY00099J]. *Analytical Methods*, *12*(10), 1324-1332. https://doi.org/10.1039/D0AY00099J

Quester, K., Avalos-Borja, M., Vilchis-Nestor, A. R., Camacho-López, M. A., & Castro-Longoria, E. (2013). SERS properties of different sized and shaped gold nanoparticles biosynthesized under different environmental conditions by

neurospora crassa extract. *PloS One*, *8*(10), e77486. https://doi.org/10.1371/journal.pone.0077486

Rashidipour, M., Maleki, A., Kordi, S., Birjandi, M., Pajouhi, N., Mohammadi, E., Heydari, R., Rezaee, R., Rasoulian, B., & Davari, B. (2019). Pectin/chitosan/tripolyphosphate nanoparticles: Efficient carriers for reducing soil sorption, cytotoxicity, and mutagenicity of paraquat and enhancing its herbicide activity. *Journal of Agricultural and Food Chemistry*, *67*(20), 5736-5745. https://doi.org/10.1021/acs.jafc.9b01106

Rodríguez-Lorenzo, L., Álvarez-Puebla, R. A., de Abajo, F. J. G., & Liz-Marzán, L. M. (2010). Surface enhanced Raman scattering using star-shaped gold colloidal nanoparticles. *The Journal of Physical Chemistry C*, *114*(16), 7336-7340. https://doi.org/10.1021/jp909253w

Rodríguez-Lorenzo, L., Álvarez-Puebla, R. A., Pastoriza-Santos, I., Mazzucco, S., Stéphan, O., Kociak, M., Liz-Marzán, L. M., & García de Abajo, F. J. (2009). Zeptomol detection through controlled ultrasensitive surface-enhanced Raman scattering. *Journal of the American Chemical Society*, *131*(13), 4616-4618. https://doi.org/10.1021/ja809418t

Schreinemachers, P., Grovermann, C., Praneetvatakul, S., Heng, P., Nguyen, T. T. L., Buntong, B., Le, N. T., & Pinn, T. (2020). How much is too much? Quantifying pesticide overuse in vegetable production in Southeast Asia. *Journal of Cleaner Production*, *244*, 118738. https://doi.org/https://doi.org/10.1016/j.jclepro.2019.118738

Sétif, P. (2015). Electron-transfer kinetics in cyanobacterial cells: Methyl viologen is a poor inhibitor of linear electron flow. *Biochimica et Biophysica Acta (BBA) - Bioenergetics*, *1847*(2), 212-222. https://doi.org/https://doi.org/10.1016/j.bbabio.2014.10.008

Shackman, H. M., Ding, W., & Bolgar, M. S. (2015). A novel route to recognizing quaternary ammonium cations using electrospray mass spectrometry. *Journal of the American Society for Mass Spectrometry*, *26*(1), 181-189. https://doi.org/10.1007/s13361-014-1019-4

Sharma, B., Frontiera, R. R., Henry, A.-I., Ringe, E., & Van Duyne, R. P. (2012). SERS: Materials, applications, and the future. *Materials Today*, *15*(1), 16-25. https://doi.org/https://doi.org/10.1016/S1369-7021(12)70017-2

Sharma, K., & Paradakar, M. (2010). The melamine adulteration scandal. *Food Security*, *2*(1), 97-107. https://doi.org/10.1007/s12571-009-0048-5

Singh, R., Kumar, N., Mehra, R., Kumar, H., & Singh, V. P. (2020). Progress and challenges in the detection of residual pesticides using nanotechnology based colorimetric techniques. *Trends in Environmental Analytical Chemistry*, *26*, e00086. https://doi.org/https://doi.org/10.1016/j.teac.2020.e00086

Stosch, R., Henrion, A., Schiel, D., & Güttler, B. (2005). Surface-enhanced Raman scattering based approach for quantitative determination of creatinine in human serum. *Analytical Chemistry*, *77*(22), 7386-7392. https://doi.org/10.1021/ac0511647

Sun, L., Yu, Z., & Lin, M. (2019). Synthesis of polyhedral gold nanostars as surface-enhanced Raman spectroscopy substrates for measurement of thiram in peach

juice [10.1039/C9AN00687G]. *Analyst*, *144*(16), 4820-4825. https://doi.org/10.1039/C9AN00687G

Sun, Q., Suo, Z., Pu, H., Tang, P., Gan, N., Gan, R., Zhai, Y., Ding, X., & Li, H. (2018). Studies of the binding properties of the food preservative thiabendazole to DNA by computer simulations and nmr relaxation [10.1039/C8RA03702G]. *RSC Advances*, *8*(36), 20295-20303. https://doi.org/10.1039/C8RA03702G

Suzuki, M., Niidome, Y., Terasaki, N., Inoue, K., Kuwahara, Y., & Yamada, S. (2004). Surface-enhanced nonresonance Raman scattering of rhodamine 6G molecules adsorbed on gold nanorod films. *Japanese Journal of Applied Physics*, *43*(No. 4B), L554-L556. https://doi.org/10.1143/jjap.43.l554

Tiwari, V. S., Oleg, T., Darbha, G. K., Hardy, W., Singh, J. P., & Ray, P. C. (2007). Non-resonance SERS effects of silver colloids with different shapes. *Chemical Physics Letters*, *446*(1), 77-82. https://doi.org/https://doi.org/10.1016/j.cplett.2007.07.106

Tsen, C.-M., Yu, C.-W., Chuang, W.-C., Chen, M.-J., Lin, S.-K., Shyu, T.-H., Wang, Y.-H., Li, C.-C., Chao, W.-C., & Chuang, C.-Y. (2019). A simple approach for the ultrasensitive detection of paraquat residue in adzuki beans by surface-enhanced Raman scattering [10.1039/C8AN01845F]. *Analyst*, *144*(2), 426-438. https://doi.org/10.1039/C8AN01845F

Vagenas, N. V., Gatsouli, A., & Kontoyannis, C. G. (2003). Quantitative analysis of synthetic calcium carbonate polymorphs using FT-IR spectroscopy. *Talanta*, *59*(4), 831-836. https://doi.org/10.1016/s0039-9140(02)00638-0

Vian, A., Davies, E., Gendraud, M., & Bonnet, P. (2016). Plant responses to high frequency electromagnetic fields. *BioMed Research International*, *2016*, 1830262. https://doi.org/10.1155/2016/1830262

Wesselink, A. K., Hatch, E. E., Rothman, K. J., Willis, S. K., Orta, O. R., & Wise, L. A. (2020). Pesticide residue intake from fruits and vegetables and fecundability in a North American preconception cohort study. *Environment International*, *139*, 105693. https://doi.org/https://doi.org/10.1016/j.envint.2020.105693

Willets, K. A., & Van Duyne, R. P. (2007). Localized surface plasmon resonance spectroscopy and sensing. *Annual Review of Physical Chemistry*, *58*, 267-297. https://doi.org/10.1146/annurev.physchem.58.032806.104607

Winter, C. K., & Katz, J. M. (2011). Dietary exposure to pesticide residues from commodities alleged to contain the highest contamination levels. *Journal of Toxicology*, *2011*, 589674-589674. https://doi.org/10.1155/2011/589674

Wu, H., Luo, Y., Hou, C., Huo, D., Zhou, Y., Zou, S., Zhao, J., & Lei, Y. (2019). Flexible bipyramid-AuNPs based sers tape sensing strategy for detecting methyl parathion on vegetable and fruit surface. *Sensors and Actuators B: Chemical*, *285*, 123-128. https://doi.org/https://doi.org/10.1016/j.snb.2019.01.038

Xu, C., Liu, J., Bi, Y., Ma, C., Bai, J., Hu, Z., & Zhou, M. (2020). Biomass derived worm-like nitrogen-doped-carbon framework for trace determination of toxic heavy metal lead (ii). *Analytica Chimica Acta*, *1116*, 16-26. https://doi.org/https://doi.org/10.1016/j.aca.2020.04.033

Yang, T., Zhang, Z., Zhao, B., Hou, R., Kinchla, A., Clark, J. M., & He, L. (2016). Real-time and in situ monitoring of pesticide penetration in edible leaves by surface-enhanced Raman scattering mapping. *Analytical Chemistry*, *88*(10), 5243-5250. https://doi.org/10.1021/acs.analchem.6b00320

Ye, J., Hutchison, J. A., Uji-i, H., Hofkens, J., Lagae, L., Maes, G., Borghs, G., & Van Dorpe, P. (2012). Excitation wavelength dependent surface enhanced Raman scattering of 4-aminothiophenol on gold nanorings [10.1039/C2NR11805J]. *Nanoscale*, *4*(5), 1606-1611. https://doi.org/10.1039/C2NR11805J

Yen, T.-H., Lin-Tan, D.-T., & Lin, J.-L. (2011). Food safety involving ingestion of foods and beverages prepared with phthalate-plasticizer-containing clouding agents. *Journal of the Formosan Medical Association*, *110*(11), 671-684. https://doi.org/https://doi.org/10.1016/j.jfma.2011.09.002

Yuan, Y., Panwar, N., Yap, S. H. K., Wu, Q., Zeng, S., Xu, J., Tjin, S. C., Song, J., Qu, J., & Yong, K.-T. (2017). SERS-based ultrasensitive sensing platform: An insight into design and practical applications. *Coordination Chemistry Reviews*, *337*, 1-33. https://doi.org/https://doi.org/10.1016/j.ccr.2017.02.006

Zhang, C., Guanming, S., Shen, J., & Hu, R.-f. (2015). Productivity effect and overuse of pesticide in crop production in china. *Journal of Integrative Agriculture*, *14*(9), 1903-1910. https://doi.org/https://doi.org/10.1016/S2095-3119(15)61056-5

Zheng, J., & He, L. (2014). Surface-enhanced Raman spectroscopy for the chemical analysis of food. *Comprehensive Reviews in Food Science and Food Safety*, *13*(3), 317-328. https://doi.org/10.1111/1541-4337.12062

Zhu, J., Chen, Q., Kutsanedzie, F. Y. H., Yang, M., Ouyang, Q., & Jiang, H. (2017). Highly sensitive and label-free determination of thiram residue using surface-enhanced Raman spectroscopy (SERS) coupled with paper-based microfluidics [10.1039/C7AY01637A]. *Analytical Methods*, *9*(43), 6186-6193. https://doi.org/10.1039/C7AY01637A

VITA

Min-Hui Lin was born and raised in Taiwan. She acquired her Bachelor's degree in Nutrition and Health Sciences at Taipei Medical University. After graduation, she started her career as a registered dietitian at Kang-Ning General Hospital and dedicated herself to providing medical nutrition therapies and counseling. She has traveled and worked in food service in Australia. Later, she worked with Amway Taiwan company, an affiliate of an American-based corporation. During her employment, she provided regulatory support for product launch and regulatory review for food products and marketing claims. In spring 2018, she was admitted to University of Missouri and joined Dr. Mengshi Lin's research team to pursue a Master's degree in Food Science.